RZ 3940 (# ZUR1704-011) 04/04/2017
Physical Sciences 39 pages

Research Report

Atomic Force Microscopy for Molecular Structure Elucidation

Leo Gross[1], Bruno Schuler[1*], Niko Pavliček[1], Shadi Fatayer[1], Zsolt Majzik[1], Nikolaj Moll[1], Diego Peña[2], Gerhard Meyer[1]

[1]IBM Research – Zurich
8803 Rüschlikon
Switzerland

[2]Centro de Investigación en Química Biolóxica e Materiais Moleculares (CIQUS) and
Departamento de Química Organica
Universidade de Santiago de Compostela
Santiago de Compostela, 15782
Spain

*Current address:
Molecular Foundry,
Lawrence Berkeley National Laboratory,
Berkeley, CA 94720, USA

This is the accepted version of the following article: Angewandte Chemie Int'l Edition, vol. 57, no. 15, (online, February, 2018), which has been published in final form at https://doi.org/10.1002/anie.201703509

Atomic Force Microscopy for Molecular Structure Elucidation

Leo Gross[*1], Bruno Schuler[1,3], Niko Pavliček[1], Shadi Fatayer[1], Zsolt Majzik[1], Nikolaj Moll[1], Diego Peña[2] and Gerhard Meyer[1]*

1. IBM Research – Zurich, 8803 Rüschlikon, Switzerland

2. Centro de Investigación en Química Biolóxica e Materiais Moleculares (CIQUS) and Departamento de Química Orgánica, Universidade de Santiago de Compostela. Santiago de Compostela 15782, Spain.

3. Current affiliation: Molecular Foundry, Lawrence Berkeley National Laboratory, Berkeley, CA 94720, USA

** Corresponding author: LGR@zurich.ibm.com*

Using scanning probe microscopy techniques, at low temperatures and in ultrahigh vacuum, individual molecules adsorbed on surfaces can be probed with ultrahigh resolution to determine their structure and details of their conformation, configuration, charge states, aromaticity, and the contributions of resonance structures. Functionalizing the tip of an atomic force microscope with a CO molecule enabled atomic-resolution imaging of single molecules, and measuring their adsorption geometry and bond-order relations. In addition, by using scanning tunneling microscopy and Kelvin probe force microscopy, the density of the molecular frontier orbitals and the electric charge distribution within molecules can be mapped, respectively. Combining these techniques yields a high-resolution tool for the identification and characterization of individual molecules. The single-molecule sensitivity and the possibility of atom manipulation to induce chemical reactions with the tip of the microscope open up unique applications in chemistry, and differentiate scanning probe microscopy from conventional methods for molecular structure elucidation. Besides being an aid for challenging cases in natural product identification, atomic force microscopy has demonstrated to be especially suited and powerful for the investigation of on-surface reactions and the characterization of radicals and molecular mixtures. Here we review the progress that high-resolution scanning probe microscopy with functionalized tips has made for molecular structure identification and characterization in the past years, and discuss the challenges it will face in the years to come.

1. Introduction

To date, molecular structure identification relies heavily on spectroscopic methods that measure molecular ensembles; the most powerful tools comprise nuclear magnetic resonance (NMR), mass spectrometry (MS), X-ray diffraction and ultraviolet-visible (UV-vis) spectroscopy, and these techniques will remain the gold standard for the analysis of molecules [1]. Scanning probe microscopy (SPM) based on both atomic force microscopy (AFM) [2] and scanning tunneling microscopy (STM) [3] can add valuable information for structure identification and elucidation because of their capability to resolve structures in real space and their single-molecule sensitivity. Moreover, STM and AFM are compatible with atom manipulation [4, 5], making it possible to induce chemical reactions with the tip of the microscope [6, 7, 8].

With AFM using functionalized tips in ultrahigh vacuum at low temperatures, atomic resolution can be obtained on individual molecules [9], introducing it as an alternative technique for molecular identification [10]. Importantly, AFM yields information that is complementary to the information obtained with conventional techniques and can assist those methods for product identification in challenging cases [11]. AFM has less stringent demands in terms of the sample properties: compounds of low solubility, proton-poor or non-crystalline compounds, molecules that are unstable in solution, and tiny amounts of material can be handled [12]. The connectivity of NMR-resolved molecular moieties can be accessed relatively well by AFM. Moreover, AFM and STM are always applied to characterize molecules adsorbed on surfaces. So in this regard, they yield complementary information to many conventional techniques that often characterize molecules in solutions or in crystals.

Furthermore, SPM offers the possibility of atom manipulation [4, 5], for example to induce chemical reactions on surfaces [6, 7, 8, 13, 14]. As we will review here, atom manipulation can be used for the creation of novel molecules and radicals, enabling their characterization *in situ*. Moreover, AFM is well-suited for the investigation of molecules and two-dimensional structures that are created by on-surface synthesis. Most importantly, AFM allows the characterization of individual molecules. Therefore, complex molecular mixtures can be characterized molecule by molecule, isolating and identifying individual constituents. In this way, we can gain insight into the molecular architecture of such mixtures, reveal their formation processes and reaction pathways, and identify the products generated.

Besides atomic and intra-molecular resolution, AFM also yields detailed insights into molecular properties, such as the adsorption geometry and bond order; moreover, STM and Kelvin probe force microscopy (KPFM) provide information about molecular frontier orbitals and intramolecular charge distributions, respectively. Combining AFM, STM and KPFM, one can obtain details about the structure, conformation, configuration, charge state, and aromaticity of the molecule, and its adsorption properties.

In this review, we describe how SPM methods are employed for the identification and characterization of synthetic and natural compounds, molecular mixtures, and molecules created by on-

surface synthesis and atom manipulation. We also discuss the prospects and challenges of this technique for molecular structure elucidation.

2. Experiment

Atomic force microscopy (AFM) was introduced in 1986 by Binnig, Quate and Gerber [2], who received the Kavli Prize in Nanotechnology in 2016 for their invention. A large variety of different AFM operating modes and numerous AFM offsprings have since been developed, and AFM is applied in many different environments, contexts and for different purposes [15, 16, 17, 18]. In this review, we focus on atomic-resolution imaging of molecules [9]. For this purpose, AFM is typically employed in ultrahigh vacuum, at low temperature, in non-contact mode using frequency modulation [19], at constant height, with CO-functionalized tips [20, 9], and mainly using qPlus sensors [21].

Atomic resolution on molecules by AFM was first demonstrated on pentacene using a CO-functionalized tip [9], as shown in Figure 1. This experiment and all other results shown in this review were carried out or obtained in ultrahigh vacuum, of about $p = 10^{-10}$ mbar, and at low temperature, of about $T = 5$ K, ensuring very clean and very stable conditions. The setup used in our group is home-built [22], but similar commercial systems are available. The low temperature is maintained by using a He bath cryostat. The low temperature is important for several reasons: (i) Diffusion is frozen out, thus the molecules to be studied are immobilized on the substrate, and molecules/atoms that are picked up by the tip for its functionalization are immobilized at the tip. (ii) Mechanical stability is increased, while temperature drift and thermal noise are reduced. (iii) The quality factor of the force sensor is increased. iv) The cold shields surrounding the sample improve the vacuum and thus the cleanliness of the sample. Typically, a sample can be measured for many weeks without observing any contaminations on the atomic scale if the experiment is constantly cooled with liquid helium.

Single metal crystals used as substrates are typically cleaned by sputtering and annealing cycles, and thin films might be grown on them by molecular beam epitaxy in ultrahigh vacuum, e.g. few monolayer of NaCl on Cu(111). The molecules are deposited, typically at sub-monolayer coverage on the substrate. If the sample is already cold during evaporation of the molecules, molecular diffusion can be frozen out, and consequently isolated molecules may be found on the surface. The sample can be annealed to activate on-surface diffusion and molecular self-assembly or on-surface reactions.

For non-destructive imaging with high resolution, AFM is best used in the dynamic mode, also called non-contact (NC) AFM [18]. In this mode, the cantilever holding the tip oscillates at resonance. The interaction of the tip with the sample changes the resonance frequency. The shift of the resonant frequency, Δf, is the main measurement signal in such frequency-modulation AFM [19]. A feedback circuit is used to excite the cantilever at its resonance frequency and takes care of keeping the amplitude constant. For atomic resolution imaging, where short-range forces are most important, typically oscillation amplitudes A on the order of 0.5 Å are optimal as pointed out by Giessibl [23], and were also used in the experiments presented in this review.

In general, in NC-AFM the tip height z is often adjusted to keep a constant Δf (constant-frequency shift mode) so that the tip follows the topography of the surface. However, for high-resolution imaging on molecules, it is beneficial to use the constant-height mode, i.e., there is no feedback regulation of the tip height. Compared with the constant-frequency shift mode, constant-height mode has two main advantages: (i) There is one feedback circuit fewer (the control of the tip height), enabling stabler operation and a better signal-to-noise ratio; (ii) secondly, because the frequency shift $\Delta f(z)$ is a non-monotonic function of the tip height z, it is non-trivial to establish stable feedback in the region where the slope of $\Delta f(z)$ changes its sign. Importantly, atomic resolution is typically obtained in this region, i.e., near the tip height z, where $\Delta f(z)$ has its minimum. On molecules, the tip is typically scanned parallel to the surface at a distance of about 4 Å to the molecule being investigated. The typical acquisition time for such a high-resolution AFM image of a molecule is about 10 min.

Mostly qPlus sensors [21] are used as force sensors, which have a typical resonance frequency of around 30 kHz, a force constant of about 1800 N/m, and a quality factor between 10,000 and a few 100,000 at T = 5 K. Recently, atomic resolution on molecules was also demonstrated with a length-extension resonator (Kolibri sensor) [24, 25] and with Si cantilevers [26], even at room temperature [27].

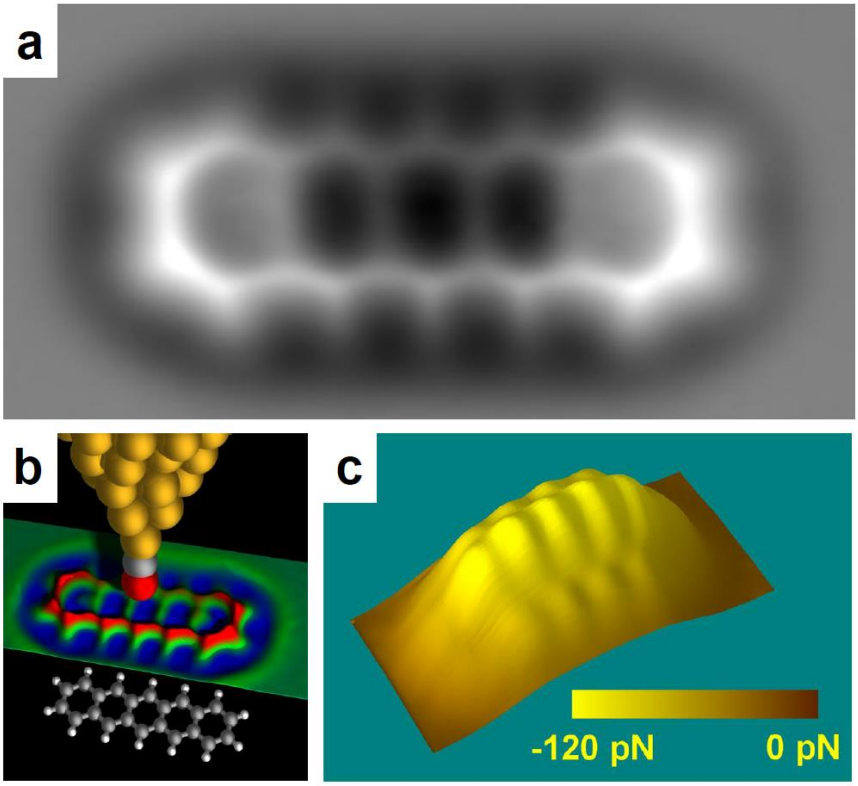

Figure 1. Pentacene imaged with CO-tip AFM. (a) Pentacene on Cu(111) imaged by constant-height non-contact AFM with a CO-functionalized tip. The color scale corresponds to Δf = -2 Hz (white) to -7 Hz (black). Resonance frequency f_0 = 23 kHz, oscillation amplitude A = 20 pm [9]. The bright features reflect regions of large electron density of the pentacene molecule, which result in repulsive force

contributions. The atomic contrast arises mainly from Pauli repulsion between tip and sample. (b) Sketch of the measurement geometry; the central colored part is a 3D representation of the measurement data [28]. (c) Forces measured in a plane above the molecule, extracted from a 3D force map. Note that the overall forces above the molecule are attractive and on the order of -100 pN. The atomic contrast results from repulsive contributions and is on the order of 10 pN. (a), (c) Adapted from [9]. Reprinted with permission from AAAS. (b) Reprinted by permission from Macmillan Publishers Ltd: Nature Chemistry [28], copyright 2011.

The chemical and physical properties of the final atoms of the tip are crucial for high-resolution imaging. Using atom manipulation, these atoms can be chosen at will, that is, individual atoms or molecules can be picked up with the tip from the surface to achieve a certain tip termination [5, 20]. Different tip functionalizations yield atomic contrast and have different benefits [9, 29]. The most popular functionalization for high-resolution AFM today is the CO tip, made by picking up a CO molecule with a metal tip [20, 9]. The CO adsorbs with its carbon atom attached to the foremost metal atom of the tip, resulting in a geometry as shown in Figure 1b. The exact geometry of the metal tip is not known (and expected to be much blunter than the tip shown in this schematic), but the last three atoms of such a tip (in this case Cu-C-O) are known. Such a CO tip is especially suited for atomic-resolution imaging because i) it has a high aspect ratio on the atomic scale; ii) it is chemically inert – enabling close distances without forming a bond to the molecule being investigated; iii) the knowledge of the atomic tip geometry facilitates interpretation and simulation, and iv) lateral deflections of the CO molecule enhance the contrast and lead to an apparent image sharpening [30, 31].

The lateral deflections result from the relatively weak lateral spring constant of the CO molecule at the tip apex, which is on the order of 0.2 N/m [30, 32]. The tilting of the CO at the tip leads to apparent distortions and results in a sharpened appearance of bonds [30]. In general, sharp features will appear at ridges in the potential energy landscape [31]. Tip relaxations also facilitate bond-order analysis [30]. However, one has to be careful as apparent bonds might arise as artefacts due to the tilting of the CO [33, 34]. These tip-relaxation effects are very well understood by now [30, 31, 34, 32, 35, 36] and can also be corrected [37]. If less distorted images are desired, other tip functionalizations, such as Xe [29], Cl [9], or CuO [38], can be used. Bond-like contrast has also been observed at the positions of hydrogen bonds using STM [39] and AFM [10, 40]. However, there is an ongoing debate whether hydrogen bonds, which feature only a very small electron density compared with covalent bonds, contribute to the STM and AFM contrast that is measured [41, 34, 42, 35, 43, 44, 45].

To date, many different tip functionalizations have been explored for AFM imaging, among them the following: (i) Functionalization with metal atoms, such as Cu, Ag, and Au, which were formed either by indenting the tip into a metal substrate or by picking up individual metal adatoms from NaCl films [46, 9, 47]. These metal tips are very reactive and tend to form bonds to the molecules under investigation before the repulsive interactions can be probed. Therefore, they usually do not achieve atomic resolution on molecules, but one can obtain submolecular contrast as demonstrated recently [48]. (ii) Functionalization with halogens, such as Cl, Br and I, which have been either extracted from thin films as in the case of Cl [46, 9] from NaCl, or dissociated from precursor molecules prior to pick-up as in the case of Br and I [29]. These tips are suited for atomic resolution imaging, and produce less strongly

distorted images than CO tips do [9]. (iii) Functionalization with noble gases, i.e., Xe [29, 49, 25] and Kr [29], which are directly picked up from the surface with the tip [5]. These tips are well suited for atomic resolution and work particularly well for adsorption geometry determination [49]. (vi) Functionalization with diatomic molecules: In addition to CO, also NO has been tested, which yields similar results as CO, but has a slightly larger lateral spring constant and is easily detached from the tip during scanning, and therefore is less preferred [29]. (v) CuO-functionalized tips, which also yield atomic resolution with less strongly distorted images than CO tips do [38]. (vi) Si- and hydrogen-passivated Si tips have also been used, even at room temperature [27]. (vii) Functionalization with larger (aromatic) molecules, such as pentacene [9], C_{60} [50, 51] and naphthalene tetracarboxylic diimide (NTCDI) [42]. Those tips can yield atomic resolution on molecules, but the interpretation is often challenging because the adsorption geometry of the molecule at the tip can lead to tips having a significant asymmetry that has to be taken into account.

Depending on the properties to be measured, other tip functionalizations than CO might be preferred. For example, Xe tips are suited for measuring the molecular adsorption geometry with high resolution [49] and also for Kelvin probe force microscopy [29]. Hapala *et al.* proposed that the electrostatic field could be probed by comparing the distortions of AFM images acquired using different tips [25] (i.e., tips with different dipole moments). Images with little distortion (but also without the apparent sharpening from tip relaxations) are obtained when using very rigid tips, such as tips functionalized with Cl [9] or CuO [38]. However, for elucidating molecular structures, CO tips are most popular, and all AFM data shown in this article have been acquired with CO-functionalized tips.

3. Molecule Characterization

3.1. The origin of atomic contrast on molecules

The measurement signal in non-contact AFM is the detuning of the cantilever's resonance, i.e., the frequency shift Δf. In the small amplitude limit, Δf is proportional to the derivative of the vertical force component. In the experiments, one can measure Δf as a function of the distance [52, 9, 53, 54, 55], also called force-distance spectroscopy, and obtain the vertical force by integration. The effect of the finite amplitude can be considered [56, 57]. To obtain images of the force above a molecule, three-dimensional maps of the frequency shift (3D force maps) are obtained. This can be done either by acquiring force-distance spectroscopy curves on a two-dimensional grid or by obtaining constant-height AFM images at different tip heights. Figure 1c shows the vertical forces extracted from a 3D force map measured above the pentacene molecule [9]. Note that the overall forces are attractive (negative) in the regime measured.

The main contrast mechanism for atomic-resolution AFM is Pauli repulsion [58]. That is, repulsive force contributions arise because the electron densities of tip and sample overlap. These repulsive contributions result in increasing frequency shifts and are observed as bright features in the constant-height AFM images above atom positions and bonds, reflecting the molecular structure. Van der Waals and electrostatic forces contribute an overall attractive background with little information on

the atomic scale and give rise to the overall attractive forces and the dark halo surrounding the molecules in AFM images [58].

The bright regions can be interpreted as positions of comparably high electron density of the molecule imaged. Importantly, for CO tips, it could be shown that lateral tip deflections induced by lateral forces lead to image distortions [30, 31]. This can be beneficial because it results in an apparent sharpening of the bonds and thus reveals a rich intra-molecular contrast [30]. However, as pointed out, one has to be careful with the interpretation because apparent bonds might arise as artifacts due to the CO tip tilting [33, 34]. These tip effects and artifacts are well characterized [30, 31, 34, 59, 32, 36] and can be corrected [37]. In addition to the Pauli repulsive forces, also the van der Waals and electrostatic forces must be considered. The electrostatic dipole of the tip has to be considered, as electrostatic forces will also have an impact on the tip deflection and thus the distortions observed [60, 61, 25]. Also the quadrupole moment that a CO tip exposes [36] is relevant for the electrostatic interaction, with higher-order multipole moments of the molecule being imaged [62].

Because of the tip deflections, it is also possible to obtain atomic-resolution images on molecules with STM using functionalized tips [63, 64, 41]. The high resolution obtained by STM is explained by the tip functionalizations acting as a force-to-current converter, that is, the tip relaxations are also observed in the tunnel current measured [64, 31, 60, 65]. Using AFM and other scanning probe methods, various properties of individual molecules can be determined, as discussed in Sections 3.2-3.5.

3.2. Adsorption geometry

Naturally, when using SPM methods, the molecules probed are adsorbed on surfaces. Molecular properties, such as their conformation, charge state, aromaticity, etc. will be influenced by their adsorption on the surface and can differ substantially from those in vacuum or in solution or on a crystal. On the one hand, we can try to minimize the interaction with the surface by using inert surfaces, for example, ultrathin layers of NaCl or Xe, in order to observe molecular properties similar to those of free molecules (see Section 4.2). However, one must always keep in mind that the results are obtained for adsorbed molecules, and care must be exercised when deducing properties of these molecules in different environments. On the other hand, the properties of adsorbed molecules play a crucial role in e.g. heterogeneous catalysis and for applications in solid-state devices. The properties of adsorbed molecules and the role of the substrate can be studied in great detail by AFM, even for individual molecules.

AFM provides an extremely accurate measurement of the adsorption geometry and conformation of individual molecules. The molecular adsorption site and in-plane orientation with respect to the substrate can be obtained by imaging both the substrate and the molecule with atomic resolution [66, 10, 49, 67], which is also possible by STM [68]. However, using AFM also the adsorption height can be measured precisely [49], which is not possible with STM because of the convolution of the topography and electronic effects. In AFM, the tip height z^* that exhibits the most negative frequency shift for a certain lateral tip position serves as a measure of the adsorption height [49]. Differences in

molecular adsorption height can be measured with an accuracy of 3 pm, and tilts of the molecular plane with respect to the substrate plane with an accuracy of 0.1° [49]. Chemisorption of molecules can be distinguished from physisorption [69]. Molecular conformations can be distinguished accurately and resolved [33, 70, 71, 72]. Moreover, also metal atoms incorporated in metal-organic complexes can be observed and localized [73, 74, 75].

The adsorption geometry of pentacene on Cu(111) is shown in Figure 2 in the map of the tip height z^*, which was extracted from a 3D force map [49]. The height z^* is the tip height z at which the frequency shift is minimal, and was determined for every lateral tip position from a $\Delta f(z)$ spectrum. The tip height z^* is a qualitatively distinct point in the $\Delta f(z)$ spectrum. It was shown that using z^*, the relative adsorption heights (i.e., the differences in molecular adsorption height) can be determined with an accuracy of 3 pm and the absolute adsorption height with an accuracy of about 20 pm. For the absolute adsorption-height measurement, the offset of z^* with respect to the bare substrate has to be calibrated on the respective substrate using a reference molecule with known adsorption height. For the determination of the adsorption geometry, Xe tips were found to yield more accurate values than CO tips, which can be explained by the larger tip relaxation of the latter [49].

As an example, pentacene was measured to adopt a curved geometry on Cu(111), with the molecular ends being slightly elevated [49]. This is also the main reason that the ends of the molecule appear brighter than the central part in the constant-height image in Figure 1a. For molecular identification, the measured adsorption geometries can serve as additional criteria to find the correct structure among different hypotheses, i.e., by comparison with calculated adsorption sites [10].

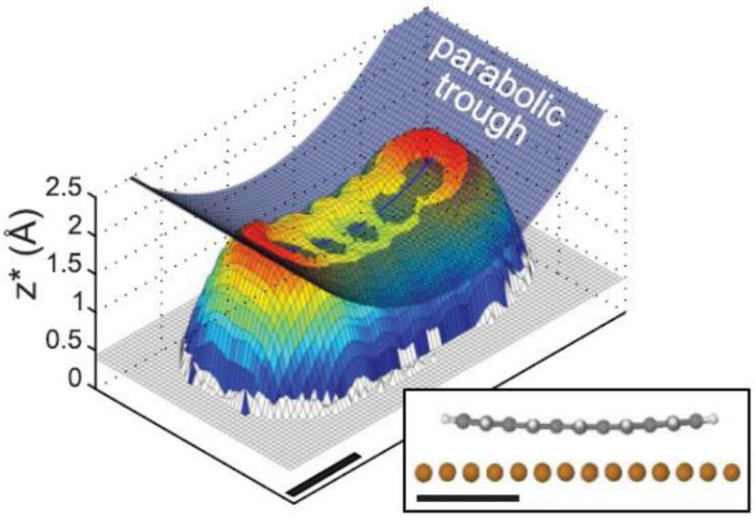

Figure 2. Adsorption geometry of pentacene on Cu(111) measured by AFM. Three-dimensional representation of z^*, i.e., the height where $\Delta f(z)$ is minimal, above pentacene on Cu(111). A parabolic through is indicated as a guide to the eye, highlighting the bent adsorption geometry that pentacene adopts on the Cu(111) surface. The inset shows a side view of the calculated molecular adsorption

geometry. Scale bars: 5 Å. Reprinted with permission from [49]. Copyright 2013 by the American Physical Society.

AFM can also be useful to determine the adsorption geometries of molecular monolayers and clusters formed by self-organization [40, 74]. In particular, AFM is suited to image weakly stable systems, e.g., to reveal the structure of water clusters on surfaces [76, 77]. To reduce the tip-sample interaction, AFM can also be performed at relatively large tip heights where the tunneling currents are too small to perform STM. Moreover, with AFM, also metal clusters, important as catalytic reaction sites, can be resolved atomically [78].

In addition to the measurement of the adsorption site and adsorption geometry, one can also laterally move the molecules or change their conformation using atom manipulation. In that case, the tip is often used to pull or push the molecules along the surface, exploiting the interaction forces between the tip and the atom/molecule that is being moved [4, 79, 80, 81] (in contrast to voltage pulses, which are applied to initiate chemical reactions by atom manipulation, as discussed in Section 4.2.). Measurements of the forces during lateral manipulation can be used to map potential energy landscapes [81] and quantify adsorption energies [82] as well as the forces needed for changing molecular conformations [83]. Recording the AFM [81, 84] and STM [79, 85, 86] signals during manipulation yields a wealth of information that can reveal details of the molecular movement during manipulation.

3.3. Bond order

Bond order is an important concept introduced by Pauling [87] to describe the stability and character of covalent bonds, which helps understanding the structure and reactivity of molecules. AFM can be considered as a privileged technique to discriminate bond orders of individual bonds experimentally [30]. Figure 3 illustrates this for the top hexagon tile of a C_{60} molecule. This hexagon features two qualitatively different C-C bonds: the bonds shared between two hexagons, labeled *h*, and the bonds shared between a hexagon and a pentagon, labeled *p*. The latter are of smaller bond order than the *h* bonds. The difference between *h* and *p* bond orders can be visualized by AFM (Figure 3b, c).

There are two contrast mechanisms to differentiate bond orders with AFM: Bonds can appear with different brightness, i.e., different frequency shifts in constant-height AFM images. Bonds of greater bond order and hence greater electron density are imaged brighter because of their greater repulsive forces. This can be seen in Figure 3b, in which the *h* bonds appear brighter than the *p* bonds. Moreover, when the tip is scanned at decreased tip height, bonds with greater bond order appear shorter, see Figure 3c. The significant differences in apparent length arise mainly due to the tilting of the CO tip [30] and provide a second mechanism to differentiate bond orders within molecules.

The bond-order-related contrast is small and often not easily deconvolved from contrast because of the non-planar adsorption geometry, different chemical elements, and different backgrounds at the edge of molecules. In the inner region of a planar molecule, the bond orders of different carbon-carbon bonds can be compared qualitatively [30]. Bond-order discrimination has been demonstrated and applied to study bond orders within polycyclic aromatic hydrocarbons [30], oligo-acetylene chains [88], and organic intermediates [89]. Using AFM, bond orders and bond lengths cannot be quantified as precisely as with the X-ray diffraction methods used on molecular crystals. However, AFM is suitable for studying bond orders of individual bonds in individual molecules adsorbed on surfaces. Therefore, the bond order can be studied in molecules made by atom manipulation [89] or in individual molecules found in molecular mixtures [88].

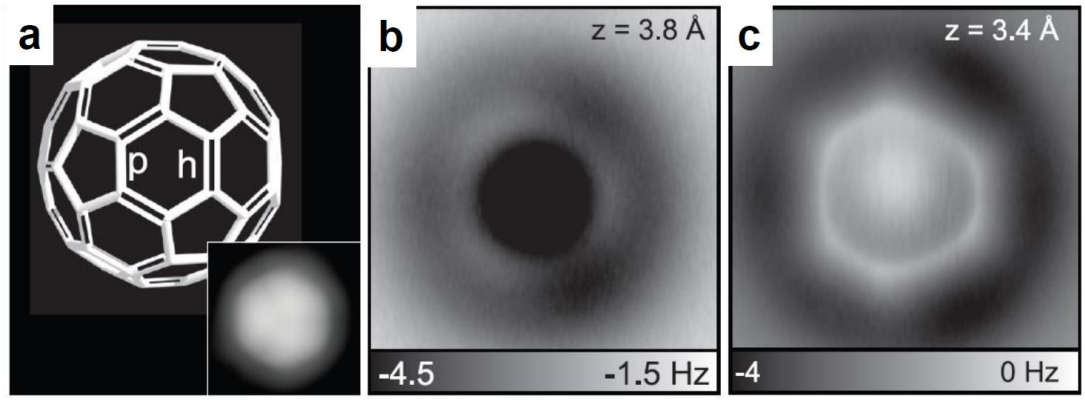

Figure 3. Bond-order discrimination in C_{60}. (a) C_{60} structural model. Bonds that are part of two hexagons, labeled *h,* are of greater bond order than bonds that are part of a pentagon and a hexagon, labeled *p*. Inset: STM image of C_{60} on Cu(111) reveals the orientation of C_{60} [90]. (b), (c) Constant-height AFM images of C_{60} on Cu(111) obtained with a CO tip at different tip heights. The tip height *z* corresponds to the estimated distance between the O atom of the CO tip and the plane of the hexagon tile of the C_{60} imaged. (b) At medium tip heights, bonds appear with different brightness, with bonds of greater bond order appearing brighter. (c) At small tip heights, bonds appear with different apparent lengths, with bonds with greater bond order appearing shorter. Adapted from [30]. Reprinted with permission from AAAS.

3.4. Charge distribution

To obtain information on the net charges and charge distributions within molecules, a special mode of AFM called Kelvin probe force microscopy (KPFM) [91], or electrostatic force microscopy, is used. KPFM is an offspring of AFM that investigates the voltage dependence of the AFM signal. In KPFM, the voltage *V* between tip and sample is varied to obtain the voltage that yields the maximum frequency shift, that minimizes the electrostatic field between tip and sample. This voltage is the main measurement signal in KPFM and is called the local contact potential difference (LCPD) [92]. Typically (in the absence of charging events), $\Delta f(V)$ takes the shape of a parabola and the peak (maximum) of the

parabola indicates the LCPD. For the idealized case of a plate capacitor, the LCPD corresponds to the contact potential difference of the two capacitor plates. However, when using a sharp probe on non-homogeneous surfaces, the LCPD can exhibit variations depending on the probe position (lateral position and tip height) on the atomic scale, hence the prefix “local”. KPFM is used for determining surface potentials and for measuring correct sample topographies with non-contact AFM because the electrostatic forces due to different contact potentials can be compensated. For a description of the working principles and applications of KPFM in general, we refer the reader to recent reviews [93, 94, 95, 96, 97]. Importantly, in the context of single molecules, KPFM can yield information about the charge states of individual atoms [98, 99] and molecules [100, 101]. Even information that reflects the charge distribution within a molecule can be obtained with sub-electron resolution [102, 103].

Qualitatively the KPFM maps can be interpreted as maps of the electrostatic field above the molecule without the presence of the tip [102, 62, 104]. Figure 4c shows a KPFM measurement above naphthalocyanine, which qualitatively resembles the calculated electrostatic field of the free molecule [102]. Naphthalocyanine features a quadrupole electrostatic moment, which is related to the position of the hydrogen atoms inside the macrocycle cavity. The molecular legs that are on the diagonal of the inner hydrogen atoms hold a positive partial charge, and the other two legs hold a negative partial charge. In a point charge model, the partial charges of this quadrupole moment correspond to about 10% of an electron’s charge, which can be clearly resolved with KPFM [102]. KPFM is sensitive to the field of the overall charge distribution, whereas AFM probes the total electron density. Atomic-resolution KPFM maps require an even longer measurement time than AFM does. For the KPFM map shown in Figure 4c, a grid of $\Delta f(V)$ spectroscopy measurements was obtained, and typical acquisition times were on the order of 10 h.

KPFM can assist in molecular structure identification. For example, a hydrogen termination can be distinguished from a fluorine termination because of the large difference in electronegativity of the two elements, which results in different electrostatic fields above the molecules [105, 59, 103]. In the future, high-resolution KPFM maps could be used to provide increased elemental sensitivity. However, the interpretation of the KPFM contrast is not always straightforward, and accompanying calculations and/or special measurement schemes are needed to exploit the full information provided by KPFM [62, 103, 106].

Because of its charge sensitivity, KPFM is particularly promising for investigating molecules featuring acceptor and donor moieties and charge-transfer complexes [105, 59, 62, 107]. KPFM is important to determine the charge state of individual molecules on surfaces and their charge-state switching. Using the tip of the microscope, the charge state of atoms and molecules can be switched by electron attachment and detachment. Different charge states can be stabilized by ionic relaxations of the substrate [108]. The resulting charge states can be determined by KPFM [98, 100, 101, 109, 110]. The charge state of a molecule can also be coupled to the oscillation of the AFM tip [111, 112], and individual electron charges can be transferred between single molecules via tip induction [101].

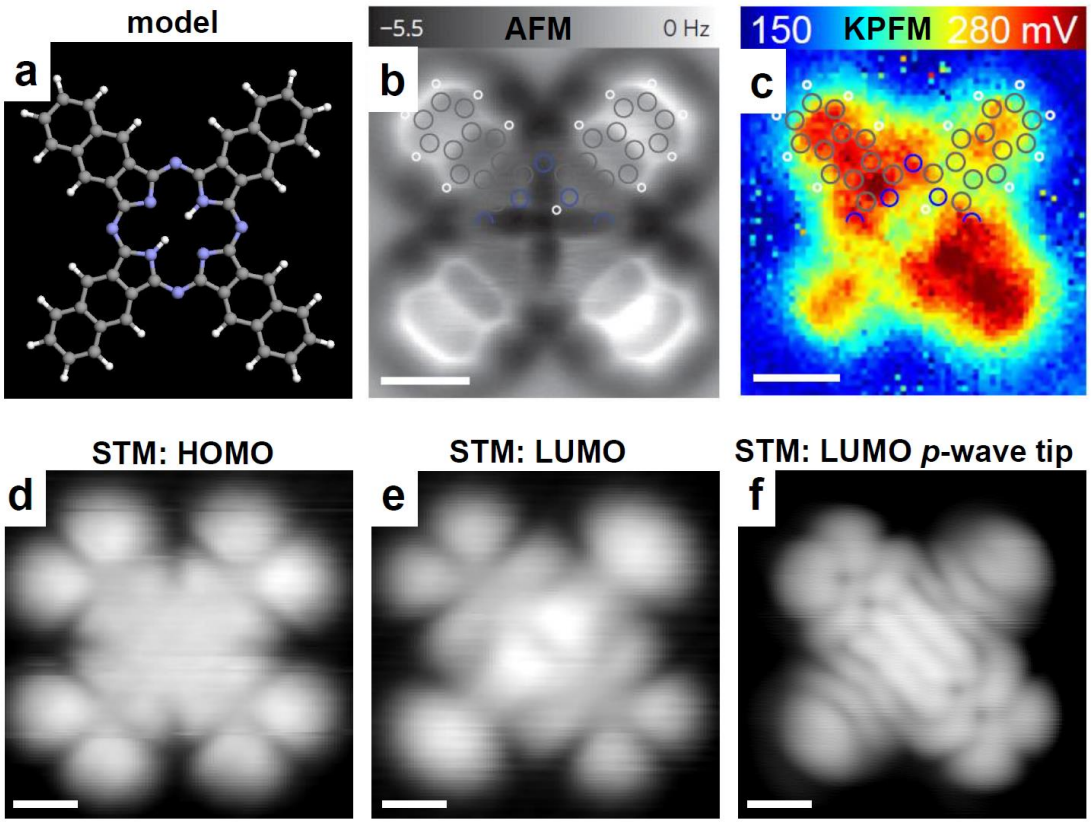

Figure 4. Atomic structure, charge distribution and molecular frontier orbitals of naphthalocyanine on bilayer NaCl on Cu(111). (a) Structural model of naphthalocyanine. (b) Naphthalocyanine imaged using CO-tip AFM [102]. (c) KPFM image, qualitatively reflecting the vertical component of the electrostatic field above the molecule [102]. (d), (e) and (f) STM images [113]. With STM, the HOMO and LUMO can be selectively imaged by choosing the corresponding bias voltage, *V*. (d) *V* = -1.6 V, (e) and (f) *V* = +0.6 V. (f) A *p*-wave tip, realized by a CO-functionalized tip, can be used to map the lateral gradient of the orbital density. Note that in all images the position of the hydrogen atoms in the center is known and corresponds to the model shown in (a). The position of the inner hydrogen atoms can be switched by the tip, triggering a tautomerization reaction [114]. In summary, AFM is sensitive to the overall electron density; KPFM is sensitive to the net charges within the molecule (including electrons and nuclei), and STM is sensitive to the density of the molecular frontier orbitals, which can be selected via the bias voltage applied. Typical acquisition times are 10 min for AFM (b), 10 h for KPFM (c), and few minutes for an STM image (d, e, f). Scale bars: 5 Å. (a), (d), (e), (f) Reprinted with permission from [113]. Copyright 2011 by the American Physical Society. (b), (c) Reprinted by permission from Macmillan Publishers Ltd: Nature Nanotechnology [102], copyright 2012.

3.5. Molecular orbitals

Using scanning tunneling microscopy (STM), the first scanning probe microscopy invented in 1982 by Binnig and Rohrer at IBM – Research Zurich [3], yet another molecular property can be

accessed. In STM, a voltage *V* is applied between tip and sample, and the resulting tunneling current is measured. For small tip-sample distances (few Å), electrons can tunnel through the junction between tip and sample, even though they are classically forbidden in this region. Typically, images are recorded in constant-current mode, i.e., the tip height is controlled to maintain a given tunneling current. In STM, topographic and electronic information are convolved in a non-trivial manner. Constant-current STM images can often be interpreted as maps of constant local density of states (LDOS) [115, 116, 117, 118].

Important for the identification of molecules is that STM can acquire images of molecular orbital densities [108]. To this end, a voltage is applied that is high enough to tunnel into or out of a frontier molecular orbital. Tunneling electrons can be temporarily attached to the lowest unoccupied molecular orbital (LUMO), and an image that resembles the LUMO orbital density (the orbital wave function squared) is obtained. At opposite polarity, electrons are temporarily detached from the highest occupied molecular orbital (HOMO), and its density is obtained [108]. Also, singly occupied orbitals can be imaged and identified by STM [119]. In addition, STM can provide information about the charge state of adsorbates on ultra-thin insulating films by looking at the scattering of interface state electrons: Only charged adsorbates act as scattering centers for interface state electrons, and only positively charged adsorbates give rise to interface state localization [46].

The STM-resolved HOMO and LUMO of naphathalocyanine are shown in Figures 4d and 4e, respectively. The LUMO, exhibiting a two-fold symmetry, can be used to determine the position of the inner hydrogen atoms that can be switched by a tautomerization reaction induced by electron attachment [114].

Typically, HOMO and LUMO densities can be resolved using STM, but the accessible voltage window for tunneling is limited to a few volts around the Fermi level. Sometimes also a few molecular orbitals with energies below the HOMO [120] or above the LUMO [121] can be imaged. For orbital imaging, it is beneficial (but not mandatory [120]) to decouple the molecule electronically from the metallic substrate using a thin insulating film, e.g., a bilayer of NaCl [122, 108] or a monolayer of Xe atoms [123, 124, 114]. In Figures 4d and 4e, a metal tip was used that resembles an *s*-wave tip exhibiting a spherical wavefunction [114, 113]. Interestingly, a CO tip results in a *p*-wave tip, exhibiting a wavefunction with a node, which yields images of the gradient of the orbital density [125] as shown for the LUMO in Figure 3f [113, 126]. Orbital imaging with a *p*-wave tip can lead to a higher resolution for orbital imaging.

4. Molecule identification

4.1. Pure compounds

The most direct application of atomically-resolved AFM imaging of molecules is the identification of pure compounds. In most cases, the structure of pure compounds can be deduced by conventional methods for structure identification, for example, by nuclear magnetic resonance (NMR), mass spectrometry (MS), infrared spectroscopy (IR) and in addition, if applicable, UV-vis spectroscopy

and X-ray crystallography [1, 127]. Here AFM has a niche application as a complementary method in those cases where the conventional techniques are not sufficient for an unambiguous identification. Challenges for conventional methods can arise if the compound is poorly soluble, difficult to purify, if only a small amount of material is available, if the compound is proton poor, if the molecule is unstable in solution or under ambient conditions, or if crystallization is difficult. These conditions do not really affect AFM as it does not require solubility and only small amounts of material are required (typically 100 µg to 1 mg of the material is used for analysis; we estimate that about 5 ng of material should be sufficient by optimizing the sample preparation [12]). A small H/C ratio is usually beneficial for AFM, which yields the best results on planar aromatic structures. Therefore, AFM effectively complements conventional techniques for structure elucidation.

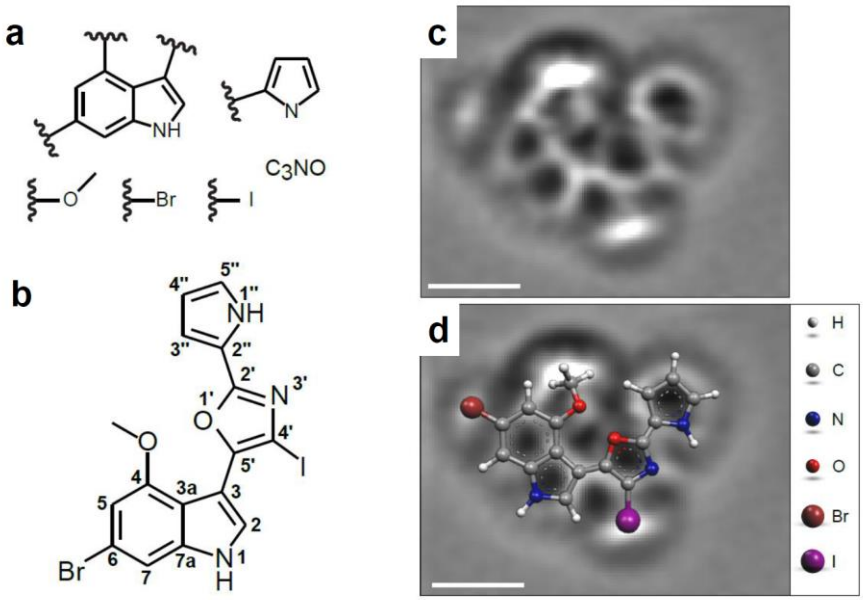

Figure 5. Identification of the natural compound breitfussin A. (a) Substructures initially derived by analysis of the spectroscopic data. (b) Molecular structure of breitfussin A. (c) AFM image of breitfussin A. (d) AFM image with the identified molecular structure overlaid. Scale bars: 5 Å. Methoxy, I and Br group could be assigned by their relative contrast in the AFM image. Adapted from [11].

In 2010 AFM was used for the first time for the identification of a natural product [10]. In the example of breitfussin A, see Figure 5, AFM was crucial for the identification of the molecule [11]. Because of the small number of hydrogens in the molecule, state-of-the-art NMR including additional computational techniques, such as computer-aided structure elucidation (CASE) and the calculation of ^{13}C NMR shifts using electronic structure calculations (DFT), could not resolve the structure. Given the limited quantity isolated, X-ray crystallography was not possible. Mass spectrometry and NMR provided

information about the fragments of the molecule, but only AFM could reveal the connection positions of the cyclic systems as well as those of the substituent groups (methoxy, Br, and I) [11, 12].

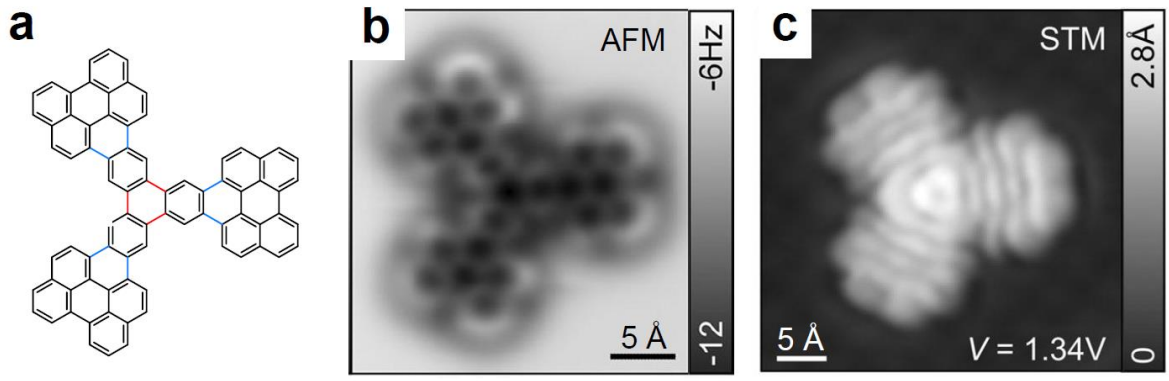

Figure 6. Identification of a synthesized compound of low solubility. (a) Structure of three-fold-symmetric 22-ring nanographene. (b) AFM image, (c) STM orbital image at a sample voltage V = 1.34 V on bilayer NaCl on Cu(111), which resolves the LUMO density. Both images were obtained with a CO tip. Combination of AFM and STM proved the successful synthesis of the molecule shown in (a). Adapted from [128].

AFM can also be important for the identification of poorly soluble compounds as in the case of the synthesized nanographene shown in Figure 6a, which features a polycyclic aromatic hydrocarbon (PAH) core of 76 sp^2 hybridized carbon atoms. Its extreme insolubility precluded purification by chromatography and characterization by conventional NMR spectroscopy. The successful synthesis of the molecule (Figure 6a) could be proved by AFM resolving the PAH core (Figure 6b). In addition, orbital imaging of the LUMO by STM (Figure 6c) confirmed the structure and indicated that the molecule is intact, with the hydrogen termination corresponding to the proposal (Figure 6a). Furthermore, owing to its single-molecule sensitivity, AFM could reveal a side product of the reaction, indicating alternative synthetic paths [128].

4.2. Molecules synthesized by atom manipulation

AFM is a key technique for the characterization of molecules that are created by on-surface synthesis because conventional methods usually cannot be applied. In most of these cases, the molecules created by on-surface synthesis also need to be characterized on the surface, which is not possible by NMR or mass spectrometry. Two different methods of on-surface synthesis can be distinguished: on-surface synthesis by heating (Section 4.3) and by atom manipulation (discussed next).

One possibility to synthesize molecules on the surface is through atom manipulation, i.e., by triggering reactions with the tip of an STM/AFM [13]. Atom manipulation was pioneered in 1990 by Eigler and Schweizer [4]. Seminal experiments demonstrating molecular dissociation and molecular synthesis by atom manipulation with STM were carried out in 1997 by Stipe et al. [6] and in 2000 by Hla et al. [7], respectively. In the latter experiment, an Ullmann coupling reaction was induced using voltage pulses from the tip, and STM and atom-manipulation experiments were used to characterize the product [7]. The improvements in atomic resolution by AFM that were achieved in the past decade, as reviewed in Section 3, enable the characterization of the reaction products with significantly better resolution, accelerating also the progress in single-molecule synthesis by atom manipulation. The technical details for triggering chemical reactions by atom manipulation are reviewed elsewhere [129]. Here we focus on the characterization of products formed by atom manipulation, describing the information that can be obtained by AFM.

Figure 7 shows an aryne molecule that has been synthesized by atom manipulation. In this case, AFM could be used to characterize the bond-order relations of the aryne molecule. Arynes are prominent reactive intermediates that only live for a very short time under ambient conditions, making their characterization extremely difficult. A precursor molecule (Figure 7a) on NaCl was dehalogenated using electron attachment from the tip to the molecular LUMO. The resulting aryne, formed after dissociation and removal of the two iodine atoms from the proximity of the molecule, is shown in Figure 7b. The extended planar aromatic hydrocarbon backbone of the molecule permitted a bond-order analysis by AFM [30], and the comparison with the hydrogenated reference molecule (Figure 7c) revealed the cumulenic character of the aryne generated. It was also possible to reattach two nearby iodine atoms to aryne using a voltage pulse, indicating that the reactivity of the aryne generated on the surface is preserved at cryogenic temperature [89]. This result is promising for the use of such intermediates to generate larger, more complex molecules using bond cleavage/formation by atom manipulation. This example shows that otherwise short-lived molecules can be characterized in detail by AFM, and that AFM can even reveal the predominant contributions of resonant structures.

The substrate surface, which can act as a catalyst or reaction partner, plays an extremely important role in on-surface reactions. By using inert surfaces, such as ultrathin layers of NaCl or Xe, also highly reactive molecules can be stabilized for their characterization with AFM.

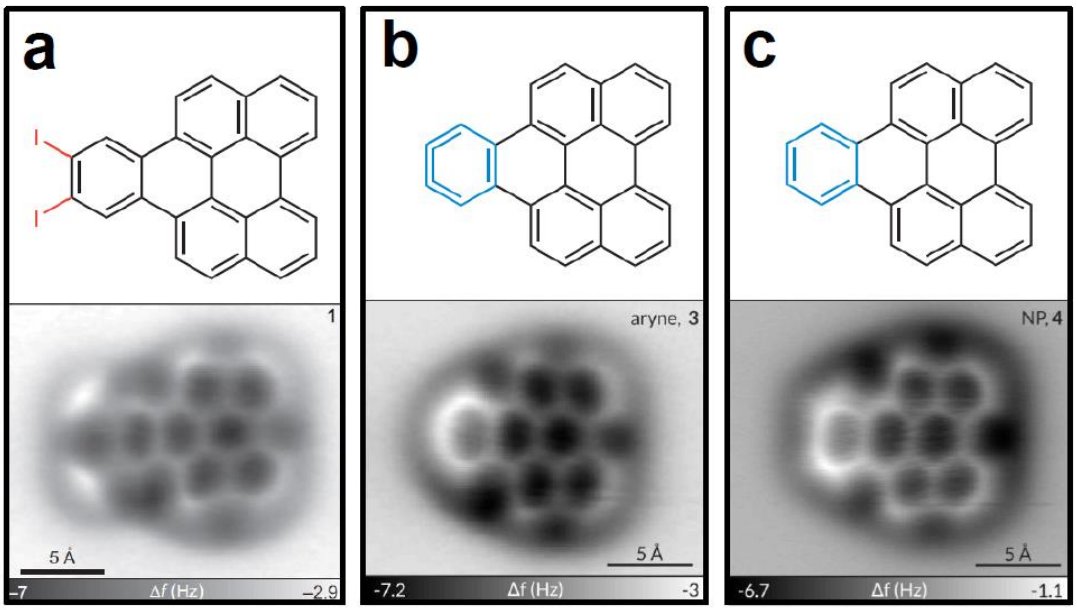

Figure 7. Aryne generation and characterization. Structures (top panels) and AFM images with CO tip (bottom panels) of (a) the precursor molecule, (b) the aryne product, formed by tip-induced iodine dissociation, and (c) the hydrogenated reference molecule. Analysis of the AFM data of the aryne molecule shown in (b) and comparison with the reference molecule shown in (c) revealed the predominant contribution of the cumulenic resonance structure for the aryne molecule. All molecules were imaged on bilayer NaCl on Cu(111). Reprinted by permission from Macmillan Publishers Ltd: Nature Chemistry [89], copyright 2015.

Atom manipulation allows the creation of molecules that cannot be synthesized using conventional chemistry. Recently, unsubstituted triangulene has been synthesized by atom manipulation for the first time. In this case, precursor molecules (Figure 8a) were dehydrogenated to form triangulene (Figure 8b) on Cu, NaCl and Xe. Triangulene is interesting because of its two unpaired electrons that form a triplet ground state. Its synthesis had been attempted by Clar and Steward in 1953 [130], but it could not be realized without stabilizing side groups until now. Using AFM, the successful generation of triangulene by atom manipulation was confirmed, and STM measurements combined with DFT calculations corroborated the open-shell character of the molecule [131]. An interesting observation is that, in contrast to intermediates that feature σ-radicals [49, 89, 132] (such as the aryne shown in Figure 7b), triangulene does not form a localized bond to the surface when adsorbed on Cu [131]. The reason for this is probably the delocalization of the unpaired electrons in triangulene, i.e., its π-radical character.

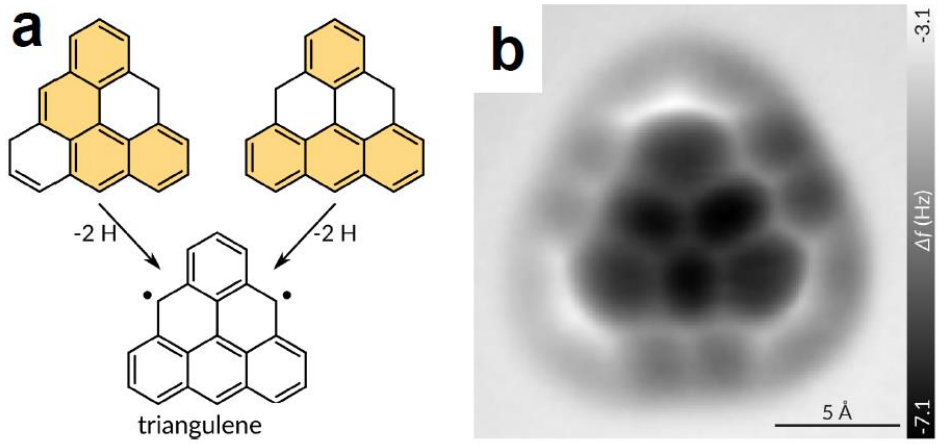

Figure 8. Generation of triangulene by atom manipulation. (a) Triangulene was generated by removing two hydrogens from precursor molecules by tip-induced voltage pulses. (b) Triangulene generated by atom manipulation and imaged by AFM with CO tip on Cu(111). Triangulene was also generated on both bilayer NaCl and monolayer Xe on Cu(111). STM orbital imaging confirmed the open-shell character of triangulene on Xe. Reprinted by permission from Macmillan Publishers Ltd: Nature Nanotechnology [131], copyright 2017.

Atom manipulation can also be used as a tool for molecular structure identification. Unknown molecules can be deliberately planarized by dissociating non-planar groups or groups that cause steric hindrance. For instance, H atoms causing steric hindrance were removed to planarize a 3D molecule so that characterization of the product and in turn identification of the initial compound became possible [133]. In addition, dehydrogenation or changing of the adsorption geometry by atom manipulation can also serve as a fingerprinting method to identify molecular moieties. An example of this is shown in Figure 9. An alkyl chain (Figure 9b) is successively oxidized (dehydrogenated) by atom manipulation (Figure 9c, d) to an alkenyl chain (Figure 9e). Thus, the characteristic contrast and distinguishing features for these sp^3- and sp^2-hybridized carbon chains are obtained, respectively. Moreover, the characteristic dehydrogenation of the alkyl chain provides another identifying feature. Similarly, the conformational switching of non-planar aliphatic rings serves as an identifier for them [71].

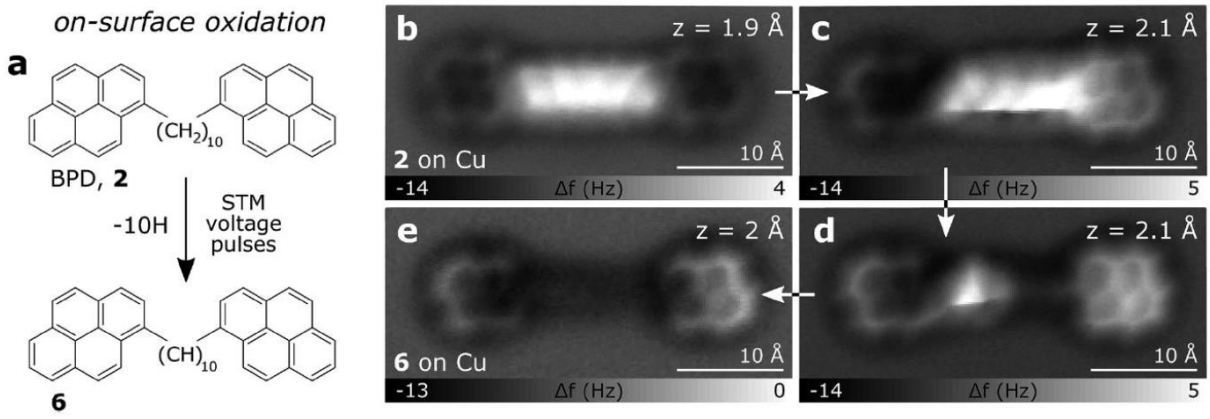

Figure 9. Imaging and tip-induced dehydrogenation of alkyl chains. An alkyl linker between two pyrene moieties has been oxidized by voltage pulses from the tip to the alkenyl chains using atom manipulation. (a) Reaction scheme. (b-e) CO-tip AFM images of (b) the molecule exhibiting a $(CH_2)_{10}$ alkyl linker chain; (c), (d) the partly oxidized molecule, and (e) oxidized to $(CH)_{10}$ alkenyl chain. All AFM measurements were performed on the same molecule on Cu(111). The tip heights *z* relate to offsets with respect to the STM setpoint of I = 2 pA and V = 0.2 V. Adapted from [71], published by The Royal Society of Chemistry.

Other subjects of intense study by atom manipulation, establishing an entire research field on their own, are molecular switches. Single molecules can exhibit a switching behavior, related to different bonds formed [114, 119, 134, 135, 136], different adsorption geometries or molecular conformations [137, 83, 138, 139, 140, 141], or different charge states [100, 142, 99, 111]. For such investigations, STM and AFM are highly suited because of their single-molecule sensitivity and the possibility to trigger switching by atom manipulation. In addition, KPFM is very useful to characterize charge-state switching as described in Section 3.4.

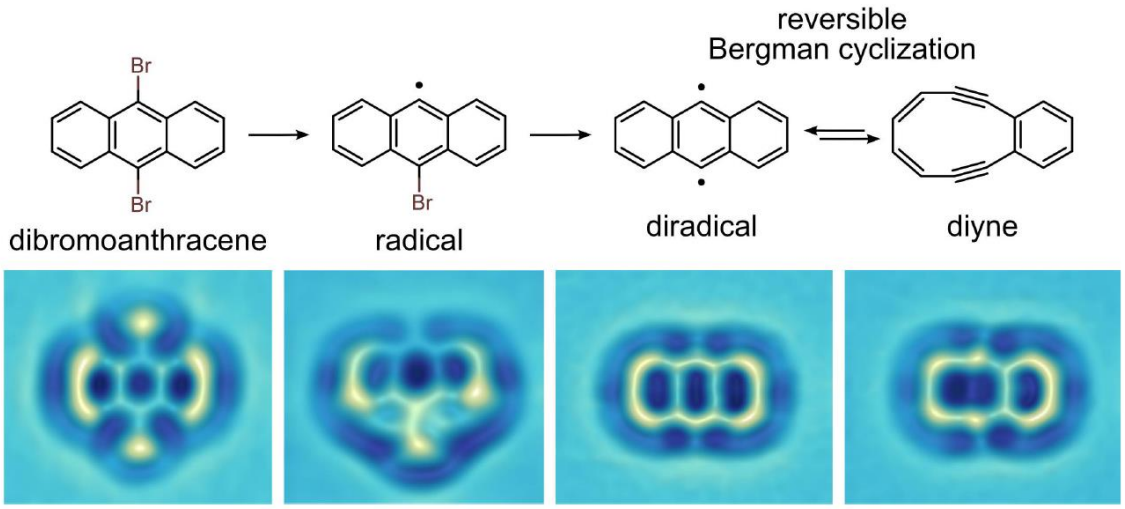

Figure 10. Reversible Bergman cyclization. Upper panel: reaction scheme; lower panel: AFM images. The Br atoms from dibromoanthracene (DBA) are dissociated to form first a radical and then a *para*-diradical. The diradical can be reversible switched into a diyne and back by tunneling electrons at $V > 1.6$ V. With an applied voltage below 1.6 V, the molecule remains stable and can be imaged by AFM (bottom panel, AFM at $V = 0$ V). All measurements were made on bilayer NaCl on Cu(111). Adapted by permission from Macmillan Publishers Ltd: Nature Chemistry [132], copyright 2016.

An example of a molecular switch, in which an internal molecular covalent carbon-carbon bond is reversibly formed and cleaved, is shown in Figure 10. Starting from a brominated precursor molecule, a *para*-diradical is formed by two successive tip-induced debromination reactions. Applying voltage pulses from the tip, the *para*-diradical can be repeatedly converted into a 10-membered ring diyne and back, constituting a reversible Bergman cyclization. Interesting for possible applications of such a molecular switch is that the spin multiplicity is changed between diradical (triplet ground state) and diyne (singlet ground state) [132].

In addition to characterizing the products using AFM, one can also directly measure the forces needed for lateral manipulation on surfaces [81], for performing conformational switching [83] or mechanical single-atom switching [143, 144], or for triggering chemical reactions of molecules [136]. Also the adsorption energies of molecules can be evaluated [82].

4.3. Molecules synthesized by on-surface heating

The second possibility for on-surface synthesis is by heating precursor molecules to form polymers and covalently bonded molecular networks as pioneered by Grill et al. [145, 146]. Graphene nanoribbons have been grown using this approach, as first achieved by Cai et al. [147]. Recently AFM has been successfully used to reveal the atomic structure of graphene nanoribbons grown by on-surface reactions [148, 149, 150, 151], see Figure 11. The atomic positions of dopant atoms within nanoribbons can be determined by AFM [149], as demonstrated in Figure 11a, where two substitutional B atoms are located in every dark region. AFM is also suitable for obtaining the edge structure of graphene nanoribbons, which, beside as arm-chair ribbons [147], have been grown and then measured using AFM with chiral (see Figure 11b) [151] and zigzag edges (see Figure 11c) [150]. Also, the connectivity of fused nanoribbons can be resolved by AFM [148, 152].

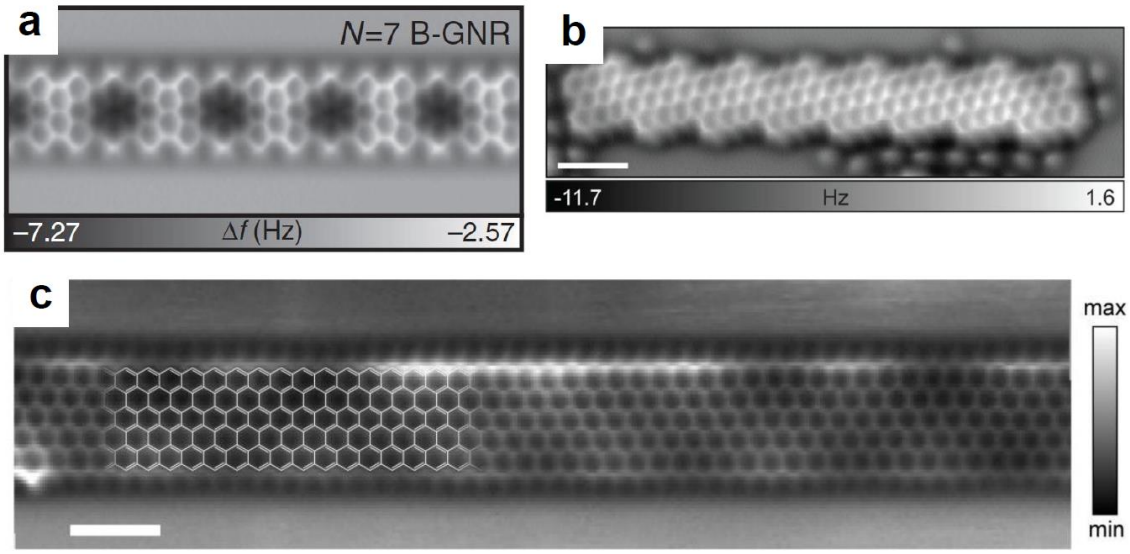

Figure 11. Characterization of graphene nanoribbons grown by on-surface synthesis. The exact structure of graphene nanoribbons formed by on-surface chemistry upon annealing of precursor molecules can be revealed by AFM. Shown here are examples for (a) boron-doped armchair graphene nanoribbons on Au(111) [149], (b) chiral graphene nanoribbons on Cu(111) [151], and (c) zigzag graphene nanoribbons on Au(111) [150]. (a) Reprinted with permission from [149]. (b) Reprinted with permission from [151], published by The Royal Society of Chemistry. (c) Reprinted by permission from Macmillan Publishers Ltd: Nature [150], copyright 2016.

Novel molecules were synthesized by heating precursor molecules on surfaces and intermediates, and the final products were determined using AFM [153, 88, 154, 155, 156, 75, 24]. A recent example is shown in Figure 12, where Kawai et al. [156] used AFM to identify different products formed by on-surface synthesis by heating. The initial molecule (Figure 12a) was deposited and imaged intact on Cu(111). Snapshots of the on-surface reaction induced by successive heating steps at increasing annealing temperatures were obtained by performing AFM characterization after each annealing step. Different cyclization reactions occurred, leading (among the other products characterized) to the intermediate shown in Figure 12b formed after heating to 470 K, and finally to the molecule shown in Figure 12c after heating to 670 K [156].

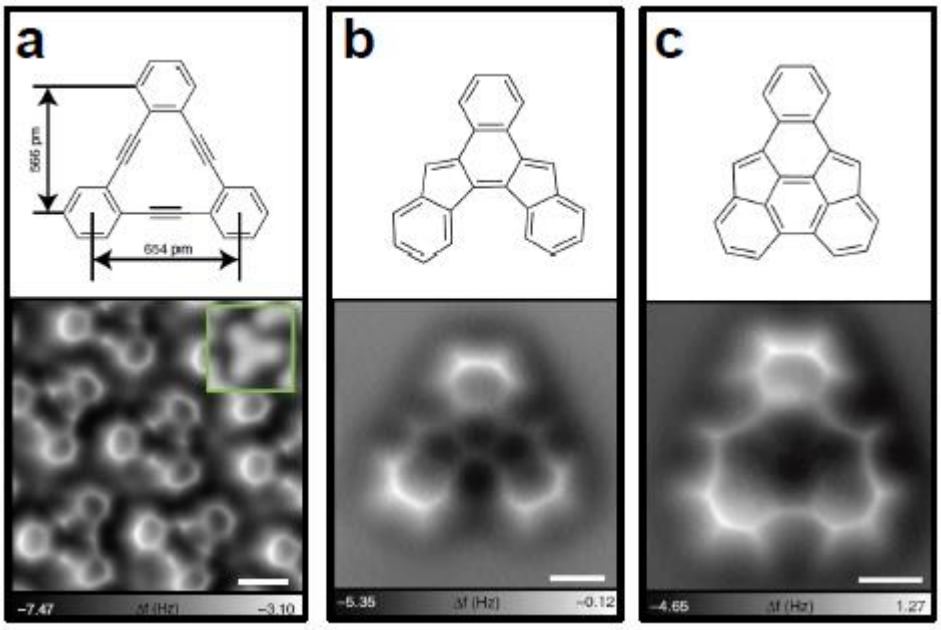

Figure 12. Structural characterization of intermediates in on-surface synthesis. Structures (top panel) and AFM images obtained with CO tip (bottom panel) of (a) the initial product, (b) an intermediate formed by heating to 470 K, and (c) the final product formed by heating to 670 K. All images were taken on Cu(111). Scale bars: 5 Å. Adapted with permission from [156].

Importantly, AFM can reveal and distinguish where intermolecular molecular bonds have formed and where not, and where metal coordination bonding has taken place [73, 74, 75]. In an experiment by Kocić et al. [75], molecular clusters were formed by heating of tetracyclic pyrazino[2,3-*f*][4,7]phenanthroline molecules on Au(111), see Figure 13. From the distance of neighboring rings, one can deduce where covalent C-C bonds between the precursor molecules had formed (indicated in red in Figure 13a) and where not (indicated in green in Fig 13a). Also, metal coordination bonding with Au atoms of the substrate could be deduced, see the structural model in Figure 13b.

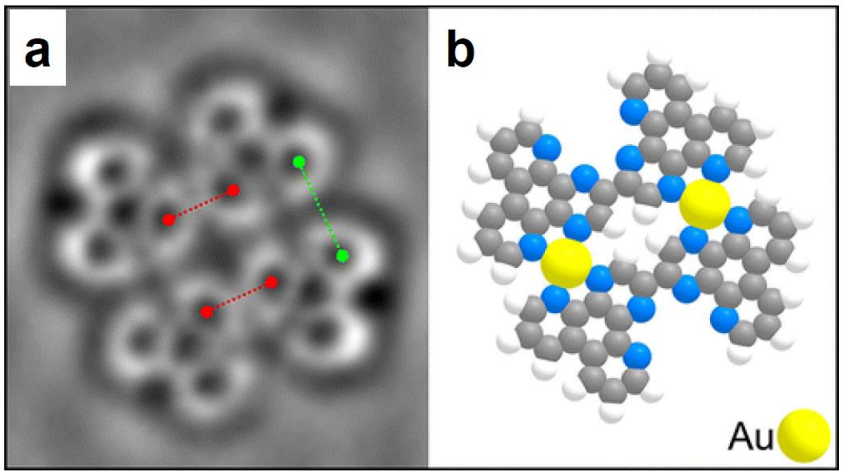

Figure 13. Characterization of on-surface coupled molecules and metal-organic coordination bonding. Molecule-metal complexes formed after annealing of tetracyclic pyrazino[2,3-*f*][4,7]phenanthroline molecules on Au(111): (a) imaged by AFM and (b) the corresponding deduced chemical structure. One can distinguish covalent C-C bond formation and deduce metal coordination bonding. Reprinted with permission from [75]. Copyright 2016 American Chemical Society.

Also the exact bonding geometry of individual molecules fused to graphene edges by on-surface reactions can be determined by AFM. He et al. [157] used AFM to reveal the bonding geometry of porphines fused by up to four C-C bonds to graphene islands on Ag(111), see Figure 14. Moreover, self-metallation of the free-base porphine to the formation of Ag-porphine could be observed (see Figure 14, column D).

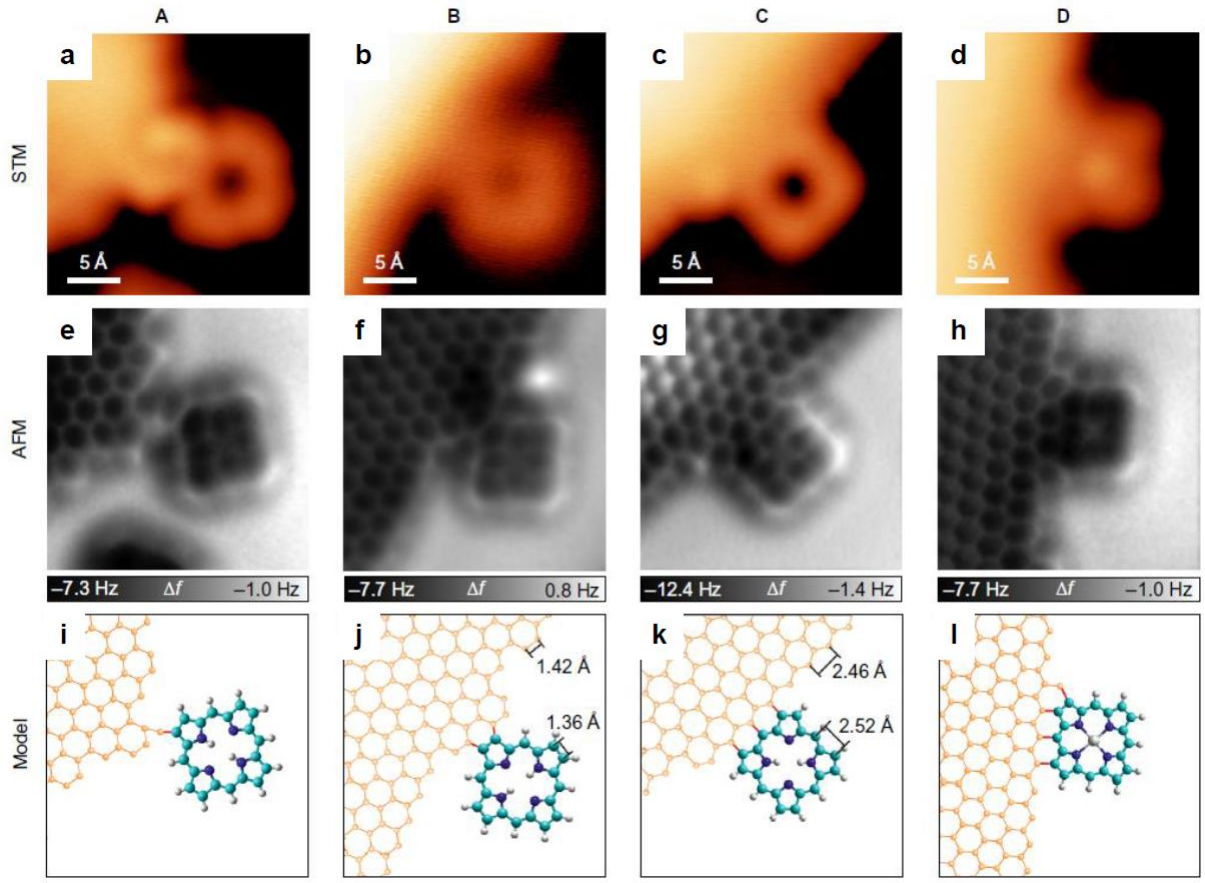

Figure 14. Characterization of tetrapyrroles coupled to graphene edges. (a-d) STM data, (e, h) AFM data, and (i-l) respective structure models formed from free-base porphines and graphene by an on-surface dehydrogenative coupling reaction on Ag(111). Porphines that formed one (column A), two (column B), three (column C) and four (column D) C-C bonds to graphene are distinguished. In columns A, B and C, the free-base core of the porphine was preserved, whereas in column D metallation to Ag-porphine could be deduced from STM and AFM data. Reprinted by permission from Macmillan Publishers Ltd: Nature Chemistry [157], copyright 2016.

The majority of those on-surface studies were performed on noble metal surfaces, but Kittelmann et al. demonstrated that covalent linking of organic molecules is even possible on bulk insulators [158, 159]. Insulating substrates are important to electronically decouple the molecular structures for possible applications. However, as STM is not applicable on bulk insulators, AFM is even more important for the characterization of molecules and networks formed on those technologically attractive substrates.

The field of on-surface synthesis is the object of intense research interest, and is expanding quickly. Several reviews describing the progress of on-surface synthesis by heating have recently been published [160, 161, 162, 163, 164].

Often the on-surface synthesis starting from a pure compound results in the formation of product mixtures because of different on-surface reaction pathways. For such diverse samples, the single-molecule sensitivity of AFM becomes extremely important as demonstrated by de Oteyza et al. [153]. AFM even allows the statistical investigation of the mixture formed based on individually resolved molecules [165, 24] as we will discuss in the next Section.

4.4. Molecular mixtures

The single-molecule sensitivity of AFM makes it a unique tool for the investigation of molecular mixtures, which can be investigated molecule by molecule. On the one hand, one obtains the structure of individual molecules forming the main constituents of the mixture being investigated. On the other hand, also side products can be observed, yielding new insights into on-surface reactions [153, 156].

Moreover, a statistical analysis is possible, quantifying the abundance of the different reaction products. An example is Figure 15, which shows different intermediates and products of an on-surface synthesis starting with the molecule in Figure 15a. The statistics of the distribution of molecules found on the surface after different annealing temperatures (see Figure 15e) yielded insight into the reaction mechanism and highlighted the contribution of selective energy dissipation and entropy in the on-surface reaction pathway as demonstrated by Riss et al. [165]. Such investigations advance our basic understanding of on-surface chemistry for the design and control of reactions at the surface of heterogeneous catalysts.

In a recent study performed by Stetsovych et al., a homochiral [7]helicene derivative was planarized by on-surface synthesis [24]. Using AFM, the intermediates and products could be identified, and it turned out that prochiral adsorbates with a pronounced non-racemic ratio were formed on-surface. Thus, the chirality of the enantiomerically pure helicene was transferred into a preferred adsorbate handedness of the prochiral molecule formed.

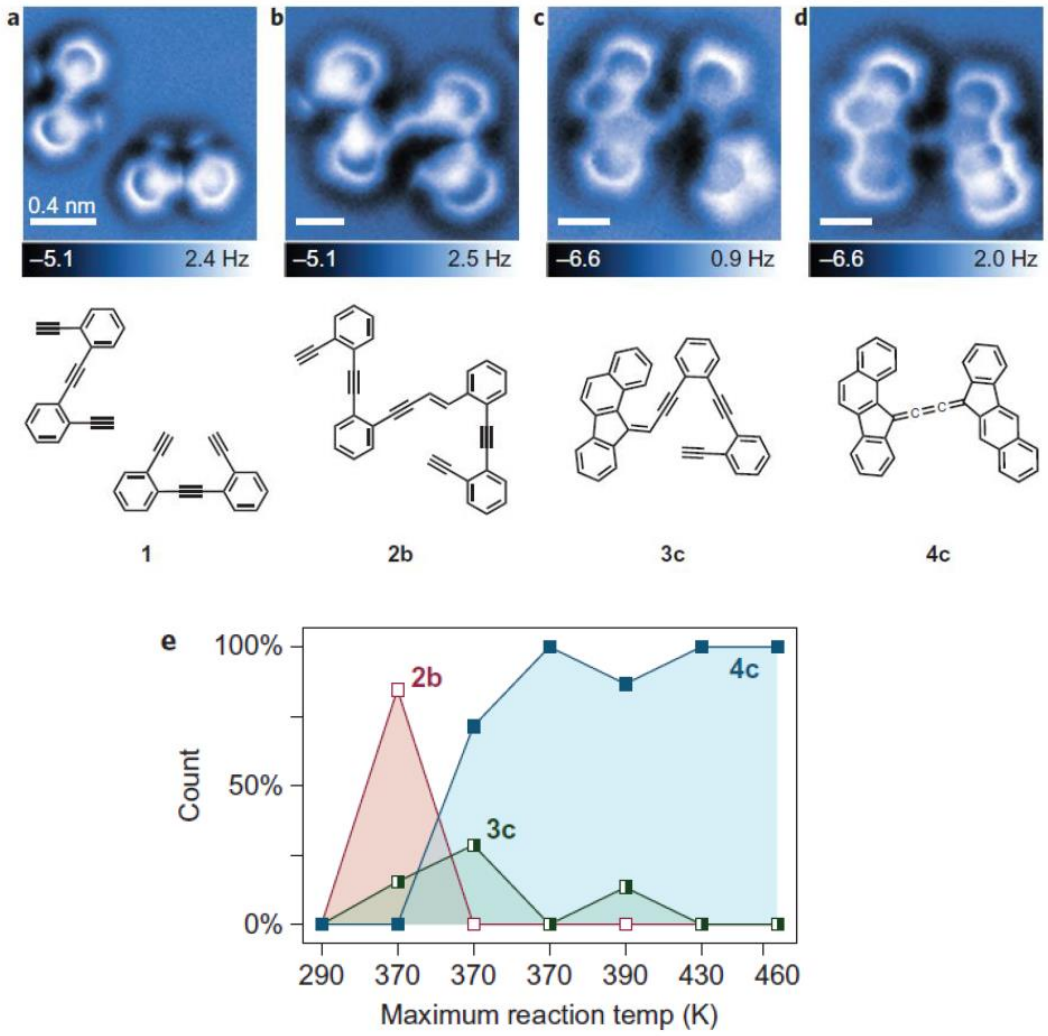

Figure 15. Structural and statistical characterization of intermediates in on-surface synthesis. AFM images of (a) the initial molecule, (b, c) intermediates, and (d) the final product obtained after annealing of 1,2-bis(2-ethynyl phenyl)ethyne (**1**) on Ag (100) to increasing maximum temperature. The statistical distribution of the molecules, identified and counted using AFM, as a function of the maximum annealing temperature is shown in (e). Reprinted by permission from Macmillan Publishers Ltd: Nature Chemistry [165], copyright 2016.

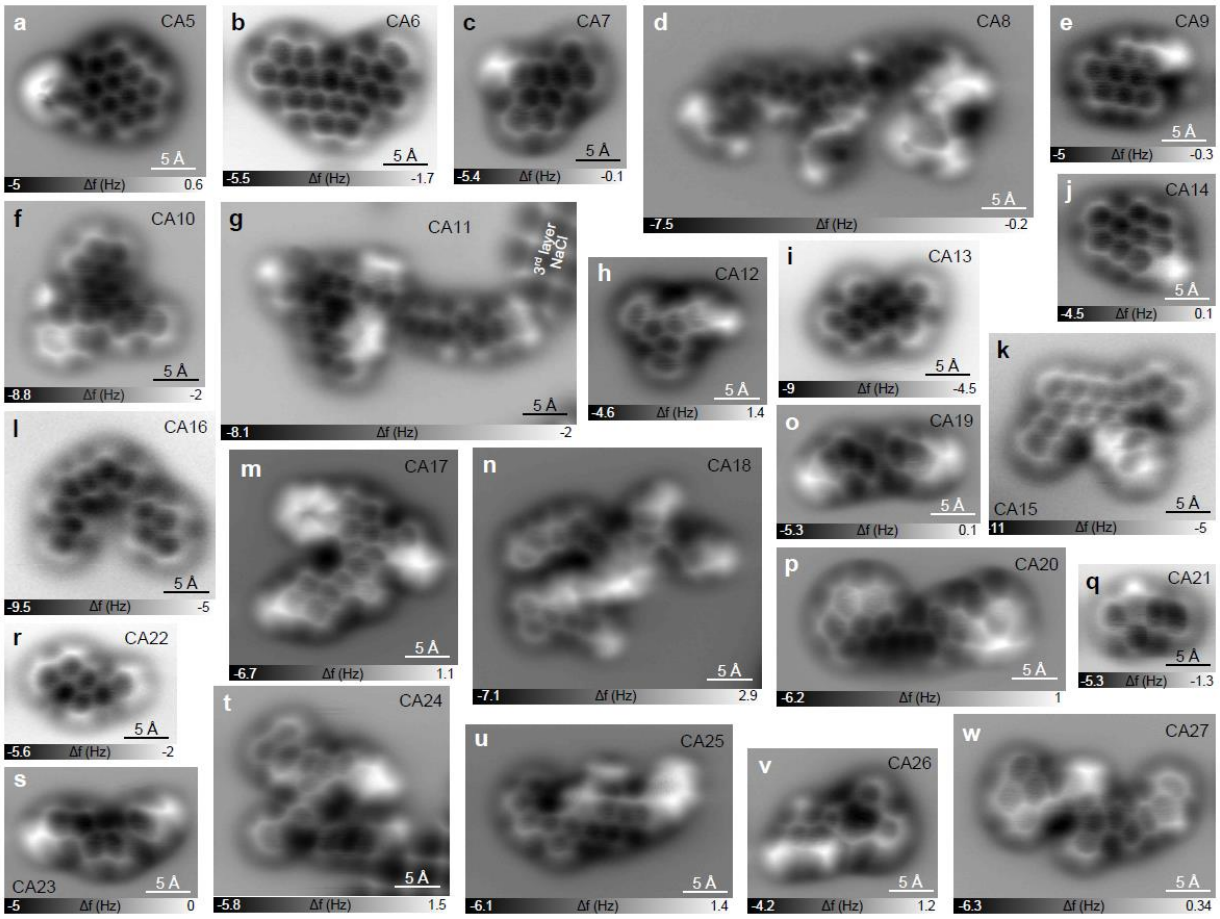

Figure 16. Characterization of complex molecular mixtures. (a)-(w) Individual molecules of coal-derived asphaltene imaged by constant-height CO-tip AFM. Analysis of the structures found by AFM provided insight into the molecular architecture of asphaltenes. Reprinted with permission from [166]. Copyright 2016 American Chemical Society.

It is also possible to investigate complex molecular mixtures found in nature by means of AFM. Among the most complex mixtures that exist are asphaltenes, the solid component of crude oil, which are of tremendous economic relevance. Such mixtures can be deposited on a surface by flash sublimation of the dry material [166].

In recent investigations of asphaltenes, more than hundred molecules could be resolved by AFM. Some results obtained on coal-derived asphaltenes, serving as a model material, are shown in Figure 16. The molecular structures identified provide a basis to understand many aspects of petroleum science, ranging from the colloidal structure and interfacial interactions to petroleum thermodynamics. Specifically, the findings contribute to resolving a long-standing debate about the molecular architecture of asphaltenes: The asphaltene molecules exhibit a very small amount of so-called archipelago-type molecules, i.e., molecules that comprise several covalently linked PAH cores. As can be observed in Figure 16, there were only very few of those (less than 10%), and the only archipelago-type molecules

found all featured a single σ-bond between the PAH cores (see e.g. Figure 16l, o). No archipelago-type molecules with connecting alkyl chains that are several $(CH)_2$ units in length, as exhibited by the custom-synthesized molecules shown in Figure 9, were observed in the asphaltene samples [166, 71].

In a very recent study [167] eight different heavy-oil-related samples of different geographic and geologic origins and different processing steps applied were investigated by AFM and STM. Each sample was characterized based on 50 to 100 individually resolved molecules. Repeating and distinguishing structural motifs could be identified by AFM, and typical molecular moieties and their relative occurrence and typical positions within the molecules were resolved. Moreover, a statistical analysis of the molecular footprints obtained by STM and the comparison of AFM data with mass spectrometry indicate the statistical significance of the sampling by AFM [167].

Especially for mixtures, AFM provides important complementary information with respect to conventional methods. Conventional methods, which are typically applied to measure the ensemble properties, provide median or mean values or distributions, e.g., the molecular weight distribution of a mixture, but an exact molecular identification of individual compounds is very challenging or even impossible. AFM, in contrast, can provide the exact molecular structure of constituents. However, AFM often cannot determine the abundance of those constituents, as the statistics that can be obtained with AFM is limited. Typical acquisition times of atomically resolved AFM images are on the order of 10 min, limiting the number of molecules that can feasibly be resolved in a sample to a few hundred.

5. Summary and outlook

AFM has become a tool that can be used to identify individual unknown molecules. It can also reveal molecular properties, such as the adsorption geometry, conformation, charge state, charge distribution and bond-order relations, and with the aid of STM also the frontier orbital densities and their occupation. For the increasing application of scanning probe microscopy in the field of molecular elucidation two unique features are key: its single-molecule sensitivity and atom manipulation. The single-molecule sensitivity allows molecular mixtures to be investigated molecule by molecule, and even rare side products can be detected. Atom manipulation opens the possibility to design and characterize novel molecules with the tip of the microscope, providing a new tool for molecule synthesis.

Several improvements could render AFM even more powerful and significantly expand its application area and its impact in molecular structure elucidation. The key goals for characterization are i) improved chemical sensitivity, ii) extension to larger and more complex molecules, and iii) improved time resolution and shorter acquisition times.

Elemental sensitivity has been demonstrated for a few elements incorporated in planar semiconductor surfaces [168, 169], but so far not on molecules, where it is extremely challenging. On molecules, the topography cannot easily be separated from chemical contrast. Non-planarity and the relatively small atom distances within the molecules render a direct elemental sensitivity extremely difficult. Moreover, atoms of the same element will exhibit different AFM contrast depending on their

hybridization, environment and oxidation state. Instead of a direct elemental identification, we think that chemical sensitivity could be established by using AFM fingerprinting of molecular subgroups. For this, a database of AFM contrasts measured on known molecular moieties could be established, providing AFM images of subgroups using different tip terminations, different tip heights, and different surfaces. Also other identifying features based, e.g., on KPFM measurements [102, 103] or atom-manipulation experiments [71] could be established. Elemental sensitivity could also be promoted by combination with other techniques, such as plasmon-enhanced Raman scattering [170].

The extension of AFM towards more complex and larger molecules faces two challenges. The first one is that large molecules must be deposited in a clean environment. To this end, deposition by electrospray ionization can be used, which is compatible with low-temperature STM/AFM, and for which the preparation of molecules having on the order of 10,000 atomic units has been demonstrated [171, 172, 173]. The second challenge is to resolve bulky, three-dimensional molecules by AFM. Methods to image the surface of non-planar molecules by atomic-resolution AFM have been successfully developed [55, 155, 26]. However, owing to the short-range forces probed in atomic-resolution AFM, the atoms of a molecule that are below its surface atomic layer are much more challenging to resolve. Smaller three-dimensional molecules might be assigned after their planarization by atom manipulation [133, 71] or by using manipulation to reveal the different facets of a molecule to the tip. Clearly, to date, AFM is most powerful on mainly planar molecules. There are large numbers of known and unknown planar molecules or molecules with planar moieties on which AFM in its current form can be applied [12].

In terms of time resolution, it would be useful to obtain AFM images faster. Currently, the acquisition time is typically on the order of 10 min for an atomically resolved constant-height image of a molecule. Since the first demonstration of AFM with atomic resolution in 2009 [9], the speed could not be improved significantly. However, sensors with much higher resonance frequency than the qPlus sensors usually employed have been demonstrated to also yield atomic resolution on molecules, e.g., the Kolibri sensor oscillating at 1 MHz [24, 25] or Si cantilevers including higher resonant modes [26]. But also with those sensors, no significant improvement in acquisition time has so far been reported. An improvement of the acquisition time of an order of magnitude would already be extremely beneficial to increase the throughput for statistical analysis of molecular mixtures, and it would allow more complex spectroscopic maps, such as 3D force spectroscopy or Δf(V) maps for KPFM, which nowadays often require acquisition times on the order of a day.

Resolving single molecular processes, such as reactions, charging, and energy transfer or spin relaxations, on the surface in real time would require a much faster time resolution, which is challenging by AFM, but might not be impossible [174]. Other methods could be compatible with AFM and benefit from the great lateral resolution of AFM. Recently, several new techniques have been developed in the field of SPM that can be used on single molecules. In the groups of Repp and Huber, electron currents induced by pump-probe terahertz laser pulses have been measured by STM, achieving femtosecond time resolution of the orbital structure of molecules [175]. In the group of Heinrich and Lutz, electron paramagnetic resonance STM has been demonstrated, which allows the measurement of spins and coherence times of individual atoms [176, 177] — a method that should be applicable to magnetic molecules in the future. Also, the detection of STM-induced luminescence of molecules has seen great

progress recently, yielding insights into the coupling and energy transfer between individual molecules [178, 179]. Combining these novel techniques with high-resolution AFM could significantly enhance our understanding of on-surface reactions and single-molecule phenomena.

Acknowledgements

We thank Rolf Allenspach for discussions. We acknowledge financial support from the European Research Council Consolidator Grant AMSEL (agreement no. 682144), the European Research Council Advanced Grant CEMAS (agreement no. 291194) and the European Union project PAMS (agreement no. 610446). DP thanks the Agencia Estatal de Investigación (MAT2016-78293-C6-3-R), the Xunta de Galicia (Centro singular de investigación de Galicia, accreditation 2016-2019, ED431G/09) and the European Regional Development Fund (ERDF) for financial support.

References

[1] R. M. Silverstein, F. X. Webster, D. J. Kiemle, D. L. Bryce, *Spectrometric identification of organic compounds*, John Wiley & Sons, **2014**.

[2] G. Binnig, C. F. Quate, C. Gerber, *Phys. Rev. Lett.* **1986**, *56*, 930–933.

[3] G. Binnig, H. Rohrer, C. Gerber, E. Weibel, *Appl. Phys. Lett.* **1982**, *40*, 178–80.

[4] D. M. Eigler, E. K. Schweizer, *Nature* **1990**, *344*, 524–526.

[5] D. M. Eigler, C. P. Lutz, W. E. Rudge, *Nature* **1991**, *352*, 600–603.

[6] B. Stipe, M. Rezaei, W. Ho, S. Gao, M. Persson, B. Lundqvist, *Phys. Rev. Lett.* **1997**, *78*, 4410–4413.

[7] S.-W. Hla, L. Bartels, G. Meyer, K.-H. Rieder, *Phys. Rev. Lett.* **2000**, *85*, 2777–2780.

[8] Y. Okawa, M. Aono, *Nature* **2001**, *409*, 683–684.

[9] L. Gross, F. Mohn, N. Moll, P. Liljeroth, G. Meyer, *Science* **2009**, *325*, 1110–1114.

[10] L. Gross, F. Mohn, N. Moll, G. Meyer, R. Ebel, W. M. Abdel-Mageed, M. Jaspars, *Nat. Chem.* **2010**, *2*, 821–825.

[11] K. O. Hanssen, B. Schuler, A. Williams, T. B. Demissie, E. Hansen, J. H. Andersen, J. Svenson, K. Blinov, M. Repisky, F. Mohn, G. Meyer, J.-S. Svendsen, R. Ruud, M. Elyashberg, L. Gross, M. Jaspars, J. Isaksson, *Angew. Chem. Int. Ed.* **2012**, *51*, 12238–12241.

[12] B. Schuler, F. Mohn, L. Gross, G. Meyer, M. Jaspars, Vol. 1, Royal Society of Chemistry, **2016**, pp. 306–320.

[13] S.-W. Hla, G. Meyer, K.-H. Rieder, *ChemPhysChem* **2001**, *2*(6), 361–366.

[14] J. I. Pascual, N. Lorente, Z. Song, H. Conrad, H.-P. Rust, *Nature* **2003**, *423*(6939), 525–528.

[15] J. Frommer, *Angew. Chem Int. Ed.* **1992**, *31*(10), 1298–1328.

[16] C. Gerber, H. P. Lang, *Nat. Nano.* **2006**, *1*, 3–5.

[17] P. Eaton, P. West, *Atomic force microscopy*, Oxford University Press, **2010**.

[18] S. Morita, F. J. Giessibl, E. Meyer, R. Wiesendanger (Eds.), *Noncontact Atomic Force Microscopy, Vol. 3*, Springer, **2015**.

[19] T. R. Albrecht, P. Grütter, D. Horne, D. Rugar, *J. Appl. Phys.* **1991**, *69*, 668–673.

[20] L. Bartels, G. Meyer, K.-H. Rieder, *Appl. Phys. Lett.* **1997**, *71*, 213–215.

[21] F. J. Giessibl, *Appl. Phys. Lett.* **1999**, *73*, 3956–3958.

[22] G. Meyer, *Rev. Sci. Instrum.* **1996**, *67*, 2960–2965.

[23] F. J. Giessibl, H. Bielefeldt, S. Hembacher, J. Mannhart, *Appl. Surf. Sci.* **1999**, *140*, 352–357.

[24] O. Stetsovych, M. Švec, J. Vacek, J. V. Chocholoušová, A. Jancark, J. Rybácek, K. Kosmider, I. G. Stará, P. Jelínek, I. Stary, *Nat. Chem.* **2017**, *9*, 213–218.

[25] P. Hapala, M. Švec, O. Stetsovych, N. J. Van Der Heijden, M. Ondrácek, J. Van Der Lit, P. Mutombo, I. Swart, P. Jelínek, *Nat. Comm.* **2016**, *7*, 11560.

[26] C. Moreno, O. Stetsovych, T. K. Shimizu, O. Custance, *Nano Lett.* **2015**, *15*, 2257–2262.

[27] K. Iwata, S. Yamazaki, P. Mutombo, P. Hapala, M. Ondrácek, P. Jelinek, Y. Sugimoto, *Nat. Comm.* **2015**, *6*, 7766.

[28] L. Gross, *Nat. Chem.* **2011**, *3*, 273–278.

[29] F. Mohn, B. Schuler, L. Gross, G. Meyer, *Appl. Phys. Lett.* **2013**, *102*, 073109.

[30] L. Gross, F. Mohn, N. Moll, B. Schuler, A. Criado, E. Guitián, D. Peña, A. Gourdon, G. Meyer, *Science* **2012**, *337*, 1326–1329.

[31] P. Hapala, G. Kichin, C. Wagner, F. S. Tautz, R. Temirov, P. Jelínek, *Phys. Rev. B* **2014**, *90*, 085421.

[32] A. J. Weymouth, T. Hofmann, F. J. Giessibl, *Science* **2014**, *343*, 1120–1122.

[33] N. Pavliček, B. Fleury, M. Neu, J. Niedenführ, C. Herranz-Lancho, M. Ruben, J. Repp, *Phys. Rev. Lett.* **2012**, *108*, 086101.

[34] S. K. Hämäläinen, N. van der Heijden, J. van der Lit, S. den Hartog, P. Liljeroth, I. Swart, *Phys. Rev. Lett.* **2014**, *113*, 186102.

[35] C.-S. Guo, X. Xin, M. A. Van Hove, X. Ren, Y. Zhao, *J. Phys. Chem. C* **2015**, *119*(25), 14195–14200.

[36] M. Ellner, N. Pavliček, P. Pou, B. Schuler, N. Moll, G. Meyer, L. Gross, R. Peréz, *Nano Lett.* **2016**, *16*, 1974–1980.

[37] M. Neu, N. Moll, L. Gross, G. Meyer, F. J. Giessibl, J. Repp, *Phys. Rev. B* **2014**, *89*, 205407.

[38] H. Mönig, D. R. Hermoso, O. Díaz Arado, M. Todorovic, A. Timmer, S. Schüer, G. Langewisch, R. Pérez, H. Fuchs, *ACS Nano* **2015**, *10*, 1201–1209.

[39] C. Weiss, C. Wagner, R. Temirov, F. S. Tautz, *J. Am. Chem. Soc.* **2010**, *132*, 11864.

[40] J. Zhang, P. Chen, B. Yuan, W. Ji, Z. Cheng, X. Qiu, *Science* **2013**, *342*, 611–614.

[41] C.-l. Chiang, C. Xu, Z. Han, W. Ho, *Science* **2014**, *344*, 885–888.

[42] A. M. Sweetman, S. P. Jarvis, H. Sang, I. Lekkas, P. Rahe, Y. Wang, J. Wang, N. R. Champness, L. Kantorovich, P. Moriarty, *Nat. Comm.* **2014**, *5*, 3931.

[43] S. Kawai, A. Sadeghi, F. Xu, L. Peng, A. Orita, J. Otera, S. Goedecker, E. Meyer, *ACS Nano* **2015**, *9*(3), 2574–2583.

[44] J. Guo, J.-T. Lü, Y. Feng, J. Chen, J. Peng, Z. Lin, X. Meng, Z. Wang, X.-Z. Li, E.-G. Wang, et al., *Science* **2016**, *352*, 321–325.

[45] S. Kawai, T. Nishiuchi, T. Kodama, P. Spijker, R. Pawlak, T. Meier, J. Tracey, T. Kubo, E. Meyer, A. S. Foster, *Sci. Adv.* **2017**, *3*(5), e1603258.

[46] J. Repp, G. Meyer, S. Paavilainen, F. E. Olsson, M. Persson, *Phys. Rev. Lett.* **2005**, *95*, 225503.

[47] L. Gross, B. Schuler, F. Mohn, N. Moll, N. Pavliček, W. Steurer, I. Scivetti, K. Kotsis, M. Persson, G. Meyer, *Phys. Rev. B* **2014**, *90*, 155455.

[48] N. Hauptmann, R. Robles, P. Abufager, N. Lorente, R. Berndt, *J. Phys. Chem. Lett* **2016**, *7*(11), 1984–1990.

[49] B. Schuler, W. Liu, A. Tkatchenko, N. Moll, G. Meyer, A. Mistry, D. Fox, L. Gross, *Phys. Rev. Lett.* **2013**, *111*, 106103.

[50] N. Hauptmann, F. Mohn, L. Gross, G. Meyer, T. Frederiksen, R. Berndt, *New J. Phys.* **2012**, *14*, 073032.

[51] C. Chiutu, A. Sweetman, A. Lakin, A. Stannard, S. Jarvis, L. Kantorovich, J. Dunn, P. Moriarty, *Phys. Rev. Lett.* **2012**, *108*, 268302.

[52] H. Hölscher, S. M. Langkat, A. Schwarz, R. Wiesendanger, *Appl. Phys. Lett.* **2002**, *81*, 4428–4430.

[53] B. J. Albers, T. C. Schwendemann, M. Z. Baykara, N. Pilet, M. Liebmann, E. I. Altman, U. D. Schwarz, *Nat. Nano.* **2009**, *4*, 307.

[54] M. Z. Baykara, T. C. Schwendemann, E. I. Altman, U. D. Schwarz, *Adv. Mater.* **2010**, *22*, 2838–2853.

[55] F. Mohn, L. Gross, G. Meyer, *Appl. Phys. Lett.* **2011**, *99*, 053106.

[56] U. Dürig, *Appl. Phys. Lett.* **1999**, *75*(3), 433–435.

[57] J. E. Sader, S. P. Jarvis, *Appl. Phys. Lett.* **2004**, *84*, 1801–1803.

[58] N. Moll, L. Gross, F. Mohn, A. Curioni, G. Meyer, *New J. Phys.* **2010**, *12*, 125020.

[59] N. Moll, B. Schuler, S. Kawai, F. Xu, L. Peng, A. Orita, J. Otera, A. Curioni, M. Neu, J. Repp, G. Meyer, L. Gross, *Nano Lett.* **2014**, *14*, 6127–6131.

[60] P. Hapala, R. Temirov, F. S. Tautz, P. Jelínek, *Phys. Rev. Lett.* **2014**, *113*, 226101.

[61] J. van der Lit, F. Di Cicco, P. Hapala, P. Jelinek, I. Swart, *Phys. Rev. Lett.* **2016**, *116*, 096102.

[62] B. Schuler, S.-X. Liu, Y. Geng, S. Decurtins, G. Meyer, L. Gross, *Nano Lett.* **2014**, *14*, 3342–3346.

[63] R. Temirov, S. Soubatch, O. Neucheva, A. C. Lassise, F. S. Tautz, *New J. Phys.* **2008**, *10*, 053012.

[64] G. Kichin, C. Weiss, C. Wagner, F. S. Tautz, R. Temirov, *J. Am. Chem. Soc.* **2011**, *133*, 16847–16851.

[65] O. Krejcí, P. Hapala, M. Ondrácek, P. Jelínek, *Physical Review B* **2017**, *95*(4), 045407.

[66] K. Lämmle, T. Trevethan, A. Schwarz, M. Watkins, A. Shluger, R. Wiesendanger, *Nano Lett.* **2010**, *10*, 2965–2971.

[67] S. Wickenburg, J. Lu, J. Lischner, H.-Z. Tsai, A. A. Omrani, A. Riss, C. Karrasch, A. Bradley, H. S. Jung, R. Khajeh, et al., *Nat. Comm.* **2016**, *7*, 13553.

[68] J. Lagoute, K. Kanisawa, S. Fölsch, *Phys. Rev. B* **2004**, *70*, 245415.

[69] W. Liu, B. Schuler, Y. Xu, N. Moll, G. Meyer, L. Gross, A. Tkatchenko, *J. Phys. Chem. Lett.* **2016**, *7*(6), 1022–1027.

[70] F. Albrecht, F. Bischoff, W. Auwärter, J. V. Barth, J. Repp, *Nano Lett.* **2016**, *16*, 7703–7709.

[71] B. Schuler, Y. Zhang, S. Collazos, S. Fatayer, G. Meyer, D. Pérez, E. Guitián, M. R. Harper, J. D. Kushnerick, D. Peña, L. Gross, *Chem. Sci.* **2017**, *8*, 2315–2320.

[72] X. Chen, S. Lei, C. Lotze, C. Czekelius, B. Paulus, K. J. Franke, *J.Chem. Phys.* **2017**, *146*, 092316.

[73] F. Albrecht, M. Neu, C. Quest, I. Swart, J. Repp, *J. Am. Chem. Soc.* **2013**, *135*, 9200–9203.

[74] Z. Yang, M. Corso, R. Robles, C. Lotze, R. Fitzner, E. Mena-Osteritz, P. Bäuerle, K. J. Franke, J. I. Pascual, *ACS Nano* **2014**, *8*(10), 10715–10722.

[75] N. Kocić, X. Liu, S. Chen, S. Decurtins, O. Krejcí, P. Jelínek, J. Repp, S.-X. Liu, *J. Am. Chem. Soc.* **2016**, *138*, 5585–5593.

[76] A. Shiotari, Y. Sugimoto, *Nat. Comm.* **2017**, *8*, 14313.

[77] J. Peng, J. Guo, P. Hapala, D. Cao, R. Ma, B. Cheng, L. Xu, M. Ondrácek, P. Jelínek, E. Wang, et al., *arXiv preprint arXiv:1703.04400.* **2017**.

[78] M. Emmrich, F. Huber, F. Pielmeier, J. Welker, T. Hofmann, M. Schneiderbauer, D. Meuer, S. Polesya, S. Mankovsky, D. Ködderitzsch, et al., *Science* **2015**, *348*, 308–311.

[79] L. Bartels, G. Meyer, K.-H. Rieder, *Phys. Rev. Lett.* **1997**, *79*, 697–700.

[80] J. A. Stroscio, R. J. Celotta, *Science* **2004**, *306*(5694), 242–247.

[81] M. Ternes, C. P. Lutz, C. F. Hirjibehedin, F. J. Giessibl, A. J. Heinrich, *Science* **2008**, *319*, 1066–1069.

[82] C. Wagner, N. Fournier, V. G. Ruiz, C. Li, K. Müllen, M. Rohlfing, A. Tkatchenko, R. Temirov, F. S. Tautz, *Nat. Comm.* **2014**, *5*, 5568.

[83] C. Loppacher, M. Guggisberg, O. Pfeiffer, E. Meyer, M. Bammerlin, R. Lüthi, R. Schlittler, J. K. Gimzewski, H. Tang, C. Joachim, *Phys. Rev. Lett.* **2003**, *90*, 066107.

[84] S. P. Jarvis, S. Taylor, J. D. Baran, N. R. Champness, J. Larsson, P. Moriarty, *Nat. Comm.* **2015**, *6*, 8338.

[85] F. Moresco, G. Meyer, K.-H. Rieder, H. Tang, A. Gourdon, C. Joachim, *Phys. Rev. Lett.* **2001**, *87*, 088302.

[86] M. Alemani, L. Gross, F. Moresco, K.-H. Rieder, C. Wang, X. Bouju, A. Gourdon, C. Joachim, *Chem. Phys. Lett.* **2005**, *402*, 180–185.

[87] L. Pauling, L. O. Brockway, J. Y. Beach, *J. Am. Chem. Soc.* **1935**, *57*, 2705–2709.

[88] A. Riss, S. Wickenburg, P. Gorman, L. Z. Tan, H.-Z. Tsai, D. G. de Oteyza, Y.-C. Chen, A. J. Bradley, M. M. Ugeda, G. Etkin, S. G. Louie, F. R. Fischer, M. F. Crommie, *Nano Lett.* **2014**, *14*, 2251–2255.

[89] N. Pavliček, B. Schuler, S. Collazos, N. Moll, D. Pérez, E. Guitián, G. Meyer, D. Peña, L. Gross, *Nat. Chem.* **2015**, *7*, 623–628.

[90] J. A. Larsson, S. D. Elliott, J. C. Greer, J. Repp, G. Meyer, R. Allenspach, *Phys. Rev. B* **2008**, *77*, 115434.

[91] M. Nonnenmacher, M. P. O'Boyle, H. K. Wickramasinghe, *Appl. Phys. Lett.* **1991**, *58*, 2921–2923.

[92] K. Wandelt, *Studies in Surface Science and Catalysis* **1987**, *32*, 280–368.

[93] V. Palermo, M. Palma, P. Samorí, *Adv. Mat.* **2006**, *18*(2), 145–164.

[94] S. Sadewasser, T. Glatzel (Eds.), *Kelvin Probe Force Microscopy*, Springer, **2011**.

[95] C. Barth, A. S. Foster, C. R. Henry, A. L. Shluger, *Adv. Mater.* **2011**, *23*, 477–501.

[96] W. Melitz, J. Shen, A. C. Kummel, S. Lee, *Surface Science Reports* **2011**, *66*(1), 1–27.

[97] Y. Miyahara, A. Roy-Gobeil, P. Grutter, *Nanotechnology* **2017**, *28*(6), 064001.

[98] L. Gross, F. Mohn, P. Liljeroth, J. Repp, F. J. Giessibl, G. Meyer, *Science* **2009**, *324*, 1428–1431.

[99] W. Steurer, J. Repp, L. Gross, I. Scivetti, M. Persson, G. Meyer, *Phys. Rev. Lett.* **2015**, *114*, 036801.

[100] T. Leoni, O. Guillermet, H. Walch, V. Langlais, A. Scheuermann, J. Bonvoisin, S. Gauthier, *Phys. Rev. Lett.* **2011**, *106*, 216103.

[101] W. Steurer, S. Fatayer, L. Gross, G. Meyer, *Nat. Comm.* **2015**, *6*, 8353.

[102] F. Mohn, L. Gross, N. Moll, G. Meyer, *Nat. Nano.* **2012**, *7*, 227–231.

[103] F. Albrecht, J. Repp, M. Fleischmann, M. Scheer, M. Ondrácek, P. Jelínek, *Phys. Rev. Lett.* **2015**, *115*, 076101.

[104] L. Gross, B. Schuler, F. Mohn, N. Moll, J. Repp, G. Meyer, Atomic Resolution on Molecules with Functionalized Tips in *Noncontact Atomic Force Microscopy* (Eds. S. Morita, F. J. Giessibl, E. Meyer, R. Wiesendanger), Springer, **2015**, Chapter 12, pp. 223–246.

[105] S. Kawai, A. Sadeghi, X. Feng, P. Lifen, R. Pawlak, T. Glatzel, A. Willand, A. Orita, J. Otera, S. Goedecker, E. Meyer, *ACS Nano* **2013**, *7*, 9098–9105.

[106] C. Wagner, M. F. Green, P. Leinen, T. Deilmann, P. Krüger, M. Rohlfing, R. Temirov, F. S. Tautz, *Phys. Rev. Lett.* **2015**, *115*, 026101.

[107] T. Meier, R. Pawlak, S. Kawai, Y. Geng, X. Liu, S. Decurtins, P. Hapala, A. Baratoff, S.-X. Liu, P. Jelinek, et al., *ACS Nano* **2017**, 10.1021/acsnano.7b03954.

[108] J. Repp, G. Meyer, S. M. Stojkovic, A. Gourdon, C. Joachim, *Phys. Rev. Lett.* **2005**, *94*, 026803.

[109] R. Pawlak, A. Sadeghi, R. Jöhr, A. Hinaut, T. Meier, S. Kawai, L. Zajac, P. Olszowski, S. Godlewski, B. Such, et al., *J. Phys. Chem. C* **2017**, *121*, 3607–3614.

[110] M. Setvin, J. Hulva, G. S. Parkinson, M. Schmid, U. Diebold, *Proc. Nat. Acad. Sci.* **2017**, *114*, E2556–E2562.

[111] N. Kocić, P. Weiderer, S. Keller, S. Decurtins, S.-X. Liu, J. Repp, *Nano Lett.* **2015**, *15*, 4406–4411.

[112] N. Kocić, S. Decurtins, S.-X. Liu, J. Repp, *J. Chem. Phys.* **2017**, *146*, 092327.

[113] L. Gross, N. Moll, F. Mohn, A. Curioni, G. Meyer, F. Hanke, M. Persson, *Phys. Rev. Lett.* **2011**, *107*, 086101.

[114] P. Liljeroth, J. Repp, G. Meyer, *Science* **2007**, *317*, 1203–1206.

[115] J. Tersoff, D. R. Hamann, *Phys. Rev. Lett.* **1983**, *50*, 1998–2001.

[116] J. Tersoff, D. R. Hamann, *Phys. Rev. B* **1985**, *31*, 805–813.

[117] C. J. Chen, *Introduction to Scanning Tunneling Microscopy*, Oxford University Press, **1993**.

[118] R. Wiesendanger, *Scanning probe microscopy and spectroscopy: methods and applications*, Cambridge University Press, **1994**.

[119] J. Repp, G. Meyer, S. Paavilainen, F. E. Olsson, M. Persson, *Science* **2006**, *312*, 1196–1199.

[120] W.-H. Soe, C. Manzano, A. De Sarkar, N. Chandrasekhar, C. Joachim, *Phys. Rev. Lett.* **2009**, *102*, 176102.

[121] J. Repp, P. Liljeroth, G. Meyer, *Nat. Phys.* **2010**, *6*, 975–979.

[122] R. Bennewitz, V. Barwich, M. Bammerlin, C. Loppacher, M. Guggisberg, A. Baratoff, E. Meyer, H.-J. Güntherodt, *Surf. Sci.* **1999**, *438*, 289–296.

[123] J. Braun, D. Fuhrmann, A. Šiber, B. Gumhalter, C. Wöll, *Phys. Rev. Lett.* **1998**, *80*, 125–128.

[124] J.-Y. Park, U. Ham, S.-J. Kahng, Y. Kuk, K. Miyake, K. Hata, H. Shigekawa, *Phys. Rev. B* **2000**, *62*(24), R16341.

[125] C. J. Chen, *Phys. Rev. B* **1990**, *42*, 8841–8857.

[126] N. Pavliček, I. Swart, J. Niedenführ, G. Meyer, J. Repp, *Phys. Rev. Lett.* **2013**, *110*, 136101.

[127] P. Crews, J. Rodriguez, M. Jaspars, *Organic Structure Analysis*, Oxford Univ. Press, **2010**.

[128] B. Schuler, S. Collazos, L. Gross, G. Meyer, D. Pérez, E. Guitián, D. Peña, *Angew. Chem. Int. Ed.* **2014**, *126*, 9150–9152.

[129] N. Pavliček, L. Gross, *Nat. Rev. Chem.* **2017**, *1*, 0005.

[130] E. Clar, D. Stewart, *J. Am. Chem. Soc.* **1953**, *75*, 2667–2672.

[131] N. Pavliček, A. Mistry, Z. Majzik, N. Moll, G. Meyer, D. J. Fox, L. Gross, *Nat. Nano.* **2017**, *12*, 308–311.

[132] B. Schuler, S. Fatayer, F. Mohn, N. Moll, N. Pavliček, G. Meyer, D. Peña, L. Gross, *Nat. Chem.* **2016**, *8*, 220–224.

[133] Z. Majzik, A. B. Cuenca, N. Pavliček, N. Miralles, G. Meyer, L. Gross, E. Fernández, *ACS Nano* **2016**, *10*, 5340–5345.

[134] F. Mohn, J. Repp, L. Gross, G. Meyer, M. S. Dyer, M. Persson, *Phys. Rev. Lett.* **2010**, *105*, 266102.

[135] T. Kumagai, F. Hanke, S. Gawinkowski, J. Sharp, K. Kotsis, J. Waluk, M. Persson, L. Grill, *Nat. Chem.* **2014**, *6*, 41–46.

[136] J. N. Ladenthin, T. Frederiksen, M. Persson, J. C. Sharp, S. Gawinkowski, J. Waluk, T. Kumagai, *Nat. Chem.* **2016**, *8*, 935–940.

[137] F. Moresco, G. Meyer, K.-H. Rieder, H. Tang, A. Gourdon, C. Joachim, *Phys. Rev. Lett.* **2001**, *86*, 672–675.

[138] L. Grill, K.-H. Rieder, F. Moresco, S. Stojkovic, A. Gourdon, C. Joachim, *Nano Lett.* **2006**, *6*, 2685–2689.

[139] M. Alemani, M. V. Peters, S. Hecht, K.-H. Rieder, F. Moresco, L. Grill, *J. Am. Chem. Soc.* **2006**, *128*, 14446–14447.

[140] R. Pawlak, S. Fremy, S. Kawai, T. Glatzel, H. Fang, L.-A. Fendt, F. Diederich, E. Meyer, *ACS Nano* **2012**, *6*, 6318–6324.

[141] V. Schendel, B. Borca, I. Pentegov, T. Michnowicz, U. Kraft, H. Klauk, P. Wahl, U. Schlickum, K. Kern, *Nano Lett.* **2015**, *16*, 93–97.

[142] I. Swart, T. Sonnleitner, J. Repp, *Nano Lett.* **2011**, *11*, 1580–1584.

[143] A. Sweetman, S. Jarvis, R. Danza, J. Bamidele, S. Gangopadhyay, G. A. Shaw, L. Kantorovich, P. Moriarty, *Phys. Rev. Lett.* **2011**, *106*, 136101.

[144] W. Steurer, B. Schuler, N. Pavliček, L. Gross, I. Scivetti, M. Persson, G. Meyer, *Nano Lett.* **2015**, *15*, 5564–5568.

[145] L. Grill, M. Dyer, L. Lafferentz, M. Persson, M. V. Peters, S. Hecht, *Nat. Nano.* **2007**, *2*, 687–691.

[146] L. Lafferentz, F. Ample, H. Yu, S. Hecht, C. Joachim, L. Grill, *Science* **2009**, *323*, 1193–1197.

[147] J. Cai, P. Ruffieux, R. Jaafar, M. Bieri, T. Braun, S. Blankenburg, M. Muoth, A. P. Seitsonen, M. Saleh, X. Feng, et al., *Nature* **2010**, *466*, 470–473.

[148] J. van der Lit, M. P. Boneschanscher, D. Vanmaekelbergh, M. Ijäs, A. Uppstu, M. Ervasti, A. Harju, P. Liljeroth, I. Swart, *Nat. Comm.* **2013**, *4*, 2023.

[149] S. Kawai, S. Saito, S. Osumi, S. Yamaguchi, A. S. Foster, P. Spijker, E. Meyer, *Nat. Comm.* **2015**, *6*, 8098.

[150] P. Ruffieux, S. Wang, B. Yang, C. Sanchez, J. Liu, T. Dienel, L. Talirz, P. Shinde, C. A. Pignedoli, D. Passerone, et al., *Nature* **2016**, *531*, 489–492.

[151] F. Schulz, P. H. Jacobse, F. F. Canova, J. van der Lit, D. Z. Gao, A. van den Hoogenband, P. Han, R. J. Klein Gebbink, M.-E. Moret, P. M. Joensuu, et al., *J. Phys. Chem. C* **2017**, *121*, 2896–2904.

[152] T. Dienel, S. Kawai, H. Söde, X. Feng, K. Müllen, P. Ruffieux, R. Fasel, O. Gröning, *Nano Lett.* **2015**, *15*, 5185–5190.

[153] D. G. de Oteyza, P. Gorman, Y.-C. Chen, S. Wickenburg, A. Riss, D. J. Mowbray, G. Etkin, Z. Pedramrazi, H.-Z. Tsai, A. Rubio, M. F. Crommie, F. R. Fischer, *Science* **2013**, *340*, 1434–1437.

[154] C. Rogers, C. Chen, Z. Pedramrazi, A. A. Omrani, H.-Z. Tsai, H. S. Jung, S. Lin, M. F. Crommie, F. R. Fischer, *Angew. Chem. Int. Ed.* **2015**, *54*, 15143–15146.

[155] F. Albrecht, N. Pavliček, N.cek, C. Herranz-Lancho, M. Ruben, J. Repp, *J. Am. Chem. Soc.* **2015**, *137*, 7424–7428.

[156] S. Kawai, V. Haapasilta, B. D. Lindner, K. Tahara, P. Spijker, J. A. Buitendijk, R. Pawlak, T. Meier, Y. Tobe, A. S. Foster, et al., *Nat. Comm.* **2016**, *7*, 12711.

[157] Y. He, M. Garnica, F. Bischoff, J. Ducke, M.-L. Bocquet, M. Batzill, W. Auwärter, J. V. Barth, *Nat. Chem.* **2016**, *9*, 33–38.

[158] M. Kittelmann, P. Rahe, M. Nimmrich, C. M. Hauke, A. Gourdon, A. Kühnle, *ACS Nano* **2011**, *5*, 8420–8425.

[159] M. Kittelmann, M. Nimmrich, R. Lindner, A. Gourdon, A. Kühnle, *ACS Nano* **2013**, *7*, 5614–5620.

[160] F. Klappenberger, Y.-Q. Zhang, J. Björk, S. Klyatskaya, M. Ruben, J. V. Barth, *Acc. Chem. Res.* **2015**, *48*, 2140–2150.

[161] R. Lindner, A. Kühnle, *Chem. Phys. Chem.* **2015**, *16*, 1582–1592.

[162] L. Talirz, P. Ruffieux, R. Fasel, *Adv. Mater.* **2016**, *28*, 6222–6231.

[163] C. Nacci, S. Hecht, L. Grill, The Emergence of Covalent On-Surface Polymerization in *On-Surface Synthesis*, Springer, **2016**, pp. 1–21.

[164] Q. Shen, H.-Y. Gao, H. Fuchs, *Nano Today* **2017**, *13*, 77–96.

[165] A. Riss, A. P. Paz, S. Wickenburg, H.-Z. Tsai, D. G. De Oteyza, A. J. Bradley, M. M. Ugeda, P. Gorman, H. S. Jung, M. F. Crommie, A. Rubio, F. R. Fischer, *Nat. Chem.* **2016**, *8*, 678–683.

[166] B. Schuler, G. Meyer, D. Peña, O. C. Mullins, L. Gross, *J. Am. Chem. Soc.* **2015**, *137*, 9870–9876.

[167] B. Schuler, S. Fatayer, G. Meyer, E. Rogel, M. Moir, Y. Zhang, M. R. Harper, A. E. Pomerantz, K. D. Bake, M. Witt, et al., *Energy & Fuels* **2017**, *31*, 6856–6861.

[168] Y. Sugimoto, P. Pou, M. Abe, P. Jelinek, R. Pérez, S. Morita, O. Custance, *Nature* **2007**, *446*, 64.

[169] J. Onoda, M. Ondrácek, P. Jelínek, Y. Sugimoto, *Nat. Comm.* **2017**, *8*, 15155.

[170] R. Zhang, Y. Zhang, Z. Dong, S. Jiang, C. Zhang, L. Chen, L. Zhang, Y. Liao, J. Aizpurua, Y. e. Luo, et al., *Nature* **2013**, *498*, 82–86.

[171] S. Rauschenbach, R. Vogelgesang, N. Malinowski, J. W. Gerlach, M. Benyoucef, G. Costantini, Z. Deng, N. Thontasen, K. Kern, *ACS Nano* **2009**, *3*, 2901–2910.

[172] C. Hamann, R. Woltmann, I.-P. Hong, N. Hauptmann, S. Karan, R. Berndt, *Rev. Sci. Instrum.* **2011**, *82*, 033903.

[173] Z. Deng, N. Thontasen, N. Malinowski, G. Rinke, L. Harnau, S. Rauschenbach, K. Kern, *Nano Lett.* **2012**, *12*, 2452–2458.

[174] Z. Schumacher, A. Spielhofer, Y. Miyahara, P. Grutter, *Appl. Phys. Lett.* **2017**, *110*, 053111.

[175] T. L. Cocker, D. Peller, P. Yu, J. Repp, R. Huber, *Nature* **2016**, *539*, 263–267.

[176] S. Baumann, W. Paul, T. Choi, C. P. Lutz, A. Ardavan, A. J. Heinrich, *Science* **2015**, *350*, 417–420.

[177] F. D. Natterer, K. Yang, W. Paul, P. Willke, T. Choi, T. Greber, A. J. Heinrich, C. P. Lutz, *Nature* **2017**, *543*(7644), 226–228.

[178] Y. Zhang, Y. Luo, Y. Zhang, Y.-J. Yu, Y.-M. Kuang, L. Zhang, Q.-S. Meng, Y. Luo, J.-L. Yang, Z.-C. Dong, et al., *Nature* **2016**, *531*, 623–627.

[179] H. Imada, K. Miwa, M. Imai-Imada, S. Kawahara, K. Kimura, Y. Kim, *Nature* **2016**, *538*, 364–367.